Modelling electro-active polymers with a dispersion-type anisotropy

Modelling electro-active polymers with a dispersion-type anisotropy

Mokarram Hossain[a,*], Paul Steinmann[b,c]

[a]*Zienkiewicz Centre for Computational Engineering, College of Engineering, Bay Campus, Swansea University, Swansea, UK*
[b]*Chair of Applied Mechanics, University of Erlangen-Nuremberg, Paul-Gordan Strasse 3, 91054 Erlangen, Germany*
[c]*School of Engineering, University of Glasgow, Glasgow G12 8QQ, United Kingdom*

Abstract

We propose a novel constitutive framework for electro-active polymers (EAPs) that can take into account anisotropy with a chain dispersion. To enhance actuation behaviour, particle-filled EAPs become promising candidates nowadays. Recent studies suggest that particle-filled EAPs, which can be cured under an electric field during the manufacturing time, do not necessarily form perfect anisotropic composites, rather they create composites with dispersed chains. Hence in this contribution, an electro-mechanically coupled constitutive model is devised that considers the chain dispersion with a probability distribution function (PDF) in an integral form. To obtain relevant quantities in discrete form, numerical integration over the unit sphere is utilised. Necessary constitutive equations are derived exploiting the basic laws of thermodynamics that result in a thermodynamically consistent formulation. To demonstrate the performance of the proposed electro-mechanically coupled framework, we analytically solve a non-homogeneous boundary value problem, the extension and inflation of an axisymmetric cylindrical tube under electro-mechanically coupled load. The results capture various electro-mechanical couplings with the formulation proposed for EAP composites.

Keywords: Electro-elasticity, electro-mechanical coupled problem, electro-active polymers (EAP), micro-sphere model, numerical integration

1. Introduction

In the recent decades, significant progress has been made on the experimental characterisation, theoretical formulations and numerical simulations of so-called smart or functional materials. The key feature of functional materials is that their important mechanical properties, e.g. various moduli, can be altered by the application of external excitations, e.g., electric fields. Among other smart materials, electro-active polymers (EAPs), capable to convert electric load into mechanical energy, attract considerable attention due to their relative low cost and potential for large actuation. They can potentially be used for actuators, sensors and even for generators [38, 77]. Moreover, they can be used as artificial muscles, see [5] for a review. The excitation of EAPs by an externally applied electric field not only results in large deformations but also a change in their internal material behaviour. Hence, the governing equations need to be solved as a coupled problem, cf. [17, 29, 78]. Two electro-mechanical forces are mainly responsible for the deformation of a polymer, cf. Vogel et al. [74]. Firstly, the so-called Maxwell stress that arises due to an electric field that

*Corresponding author. Tel.: +44-7482959957
Email addresses: mokarram.hossain@swansea.ac.uk (Mokarram Hossain), paul.steinmann@ltm.uni-erlangen.de (Paul Steinmann)

penetrates free space and matter alike. Secondly, the electrostriction that is due to intramolecular electrostatic forces of the material.

In contrast to theoretical formulations and numerical simulations of EAPs, experimental works related to either pure or composite EAPs are very rare in the literature, the work of Wissler et al. [80] is one of the few to mention. Acrylic type VHB and silicone-based polyurethane are polymeric materials that have been extensively utilised for EAP applications. Johlitz et al. [37] did a rigorous experimental characterisation of polyurethane (PU) along with numerical modelling of its time-dependent behaviour. Ask and co-workers [4] used this data to identify various mechanical material parameters for their electro-viscoelastic model. Diaconu et al. [22] studied the electro-mechanical properties of a synthesized polyurethane elastomer film-based polyester. This data is used by Ask et al. [4] to validate their electro-viscoelastic coupled model. To illustrate the time-dependent viscoelastic behaviour of VHB 4910 polymer under pure mechanical loading, a comprehensive experimental study was presented in our previous work, cf. Hossain et al. [34]. Moreover, a micro-mechanical motivated constitutive ansatz was presented to model the experimental results. Inspired by this work, a comprehensive characterization of the electromechanically coupled properties of VHB 4910 polymer is demonstrated in Hossain et al. [35]. Qiang et al. [59] presented an experimental study on the dielectric properties of a polyacrylate dielectric elastomer. They conducted an extensive study on the measurement of dielectric properties of VHB films regarding five influencing factors, i.e. pre-stretch, electrical frequency, electrode material, stress relaxation, and temperature. Ma and Cross [48] conducted an experimental investigation of electromechanical response in a dielectric acrylic elastomer in various frequency ranges at room temperature. It was concluded in the study that the electric-field-induced strain response was proportional to the square of the electric field strength up to loading of 2 MV/m. Michel et al. [49] performed a comparison between silicone and acrylic elastomers that can potentially be used as dielectric materials in electro-active polymer actuators.

Modelling electro-elasticity as well as time-dependent viscoelastic behaviour of EAPs, several research works appeared in the literature. Ask and co-workers [4] model the electrostrictive behaviour of viscoelastic polymers, particularly the electrostrictive polyurethane elastomer by a phenomenological constitutive ansatz. Büschel et al. [7] propose an electro-viscoelastic model using a multiplicative decomposition of the deformation gradient into an elastic part and a viscous part for the mechanical deformation. In this work, they consider only a time-dependent evolution for the mechanical internal variable and the electric quantity does not evolve with time. Recently, Vogel et al. [74] model the electrostrictive behaviour of viscoelastic polymers where the governing kinematical and constitutive equations are formulated in the logarithmic strain-space. In contrast to the works of Ask et al. [4] and Büschel et al. [7], Vogel et al. [74] formulated their constitutive relation considering the influence of the electric field also on the viscous response. Saxena et al. [64, 65] propose an electro-viscoelastic coupled model that additively decomposes the electric field vector in an equilibrium part and a non-equilibrium part. A multiplicative-based approach in the case of electro-elasticity is proposed by Skatulla et al. [69] which is further explored by Zäh & Miehe [84]. Thereby, the deformation gradient is decomposed into a mechanical part and an electrostrictive part. Liu et al. [86, 87, 89, 90] and Leng et al. [88] put a great amount of efforts in analysing various electro-mechanical instabilities that consider viscoelastic and temperature effects.

The finite element implementation of electro-mechanically coupled problems is an active area of research. Variational formulations for the governing equations of the coupled electro-mechanical problems are prerequisite for numerical computations in the finite element procedure. Bustamante et al. [10] and Vogel [74]

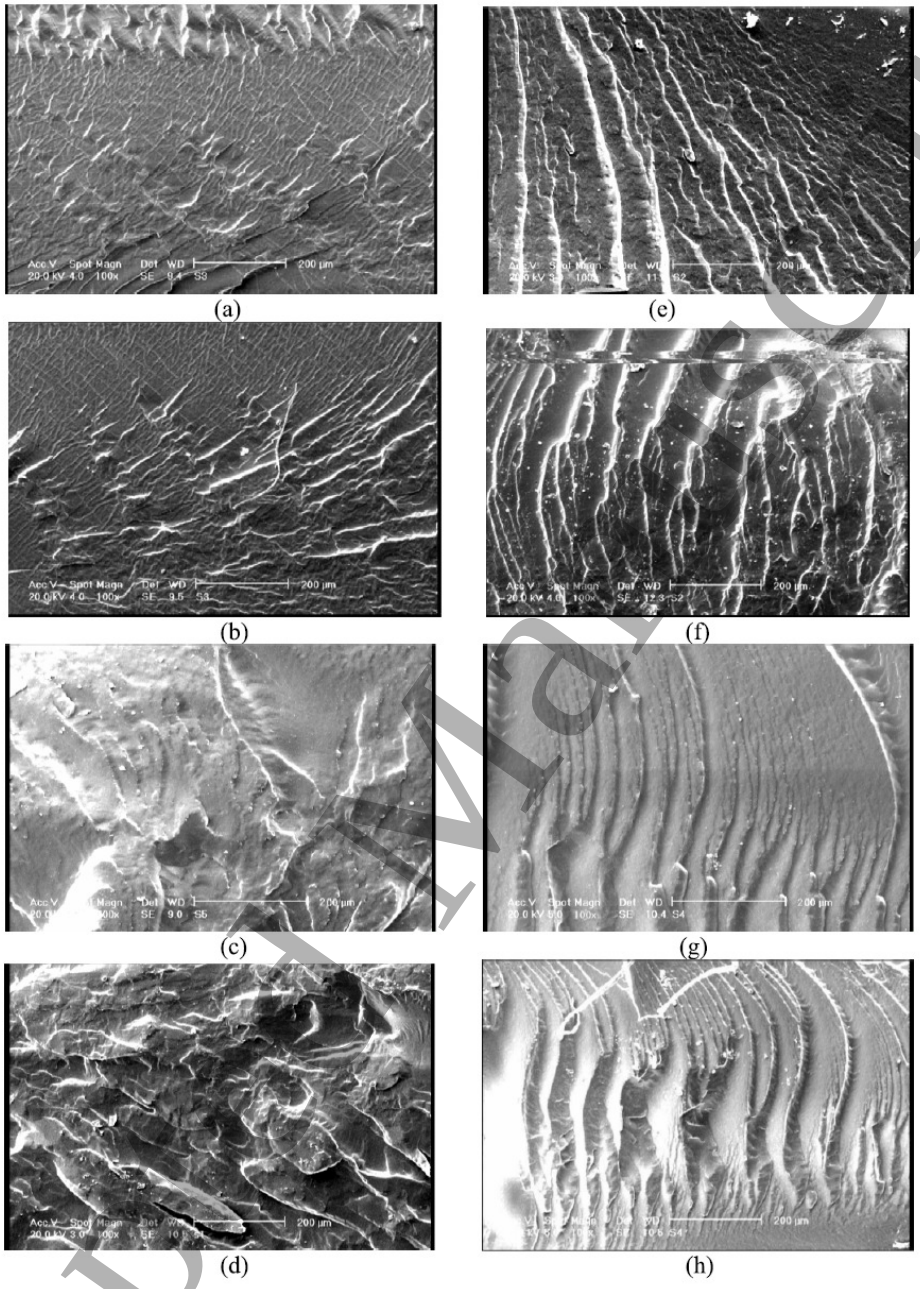

Figure 1: Scanning Electron Microscope (SEM) micrographs of fractured surfaces of silicone rubber-titania composites with random distribution of filler particles in the absence of an electric field during curing [(a)-(d)] and dielectrophoretically-assembled chain-like structure due to the application of an electric field during curing [(f)-(h)] for different concentration of titania as 2% ((a), (e)), 5% ((b), (f)), 8% ((c), (g)), and 11% ((d), (h)) (*adopted from Kashani et al.* [39], with the permission of the author)

devise variational principles where three-field formulations are proposed by considering a nearly incompressible behaviour of the bulk rubber-like materials. Gil & Ortigosa [54], Ortigosa et al. [55] in a series of papers propose a new constitutive framework with finite element implementations for large strain electromechanics based on convex multi-variable strain energies. Most of the earlier numerical formulations of EAPs neglect the free space contribution. However, very recently, Pelteret et al. [58] devise a computational framework for quasi-incompressible electro- and magneto-elastic solids immersed in free space.

One of the major drawbacks of EAPs is the requirement of a high electric voltage even for a reasonable mechanical deformation. Recent studies demonstrate that the inclusion of fillers of high dielectric permittivity into the polymeric matrix can increase the deformation induced by a reasonable voltage level, see [11, 27, 81, 82, 86, 39, 50]. To increase the dielectric permittivity of polymeric materials, several strategies are currently documented in the literature [23, 27, 81, 82, 86, 39] which can be classified into three main groups: random composites, field-structured composites, and new synthetic polymers [12]. In the case of field-structured EAPs, the fillers are used to make a composite material while the curing occurs in the presence of an externally applied electric field. As a result, the fillers usually align in the direction of the applied electric field, i.e. it helps to create a preferred direction in EAP composites, cf. Fig 1(e-h). The alignment of dipoles under the application of an electric field increases the electric polarization and hence the polarization stress [39]. More precisely, it is observed that the application of an external electric field during the curing process yields a field-structured composite where the axis of anisotropy is not perfectly defined, rather there is a chain dispersion along a mean orientation, cf. Fig 1(e-h). In the absence of an electric field during the curing process, several experimental works demonstrate the formation of filled isotropic electro-active polymeric composites with homogeneously distributed particles, see [40, 12, 82, 86, 39, 42, 60, 61, 70, 81, 82].

For the modelling of particle-reinforced EAP composites, Bustamante [9] proposes a constitutive model that considers transverse isotropy. To the best of the authors' knowledge, there is no constitutive model that can capture the chain dispersion observed in experiments of the field-structured EAP composites. In contrast, Saxena et al. [66] propose a probability based structure tensor to capture the chain-like imperfect anisotropy in the case of magneto-elasticity. Recently, Thylander [71], Thylander et al. [72] formulate a micro-sphere-based constitutive framework for electro-elasticity where the well-known Bazant & Oh [6] integration scheme is used for the numerical quadrature over the unit sphere. However, this work does not take into account the dispersed anisotropy which is experimentally observed in particle-filled EAP composites. The modelling of dispersion-type anisotropy has been an active field of research in the case of modelling biological tissues. Ideally, two types of strategies are proposed in the literature, i.e. Angular Integration (AI) based models and Generalised Structure Tensor (GST) inspired models, see [15, 16, 67, 68]. GST-based models receive popularity over AI approaches due to their simple and closed form expression. However, several studies have convincingly demonstrated that GST-based models suffer significant deficiencies in validating real experimental data in the case of biological tissues, cf. [14, 15, 16, 67, 68]. To ameliorate such drawbacks, higher order structure tensors are devised which improve the results significantly, cf. Pandolfi & Vasta [56], Pandolfi et al. [57]. Despite that, there still exist mismatches between the two approaches. Hence many authors prefer AI-based models regardless of their higher computational cost. In this contribution, we develop a constitutive framework that accounts for transversely isotropic dispersion using a probability distribution function (PDF) where the numerical integration appearing in the framework is performed on the unit sphere via suitable integration schemes. For the sake of simplicity, the time-dependent viscoelastic behaviour of the underlying polymeric matrix is discarded at this stage. Moreover, comparisons between AI-based formulations and GST-inspired models for electro-mechanically coupled problems are

left for a future investigation.

This paper is organized as follows. In Section 2, the finite strain theory of electro-elasticity is briefly reviewed where at first relevant nonlinear kinematics and balance laws in the spatial setting are illustrated followed by the material description of the same quantities. Section 3 focuses on the key contribution of the paper, i.e. a constitutive modelling of the dispersion-type transverse isotropy in electro-elasticity. Furthermore, numerical integration over the unit sphere is elucidated here followed by a short discussion on the transverse isotropic distribution function that captures the chain dispersion within the EAP composites. The final Section 4 presents an analytical example which illustrates that the proposed model can capture relevant phenomena of dispersed field-structured EAP composites under electro-mechanical loads. Section 5 concludes the paper with a summary and an outlook to future works.

2. Basics of non-linear electro-mechanics

2.1. Kinematics

In the case of large deformations we distinguish the reference configuration $\mathcal{B}_0$ from the deformed configuration $\mathcal{B}_t$. The body $\mathscr{B}$ is composed by an infinite and continuous set of points. The placement of these points in the reference configuration $\mathcal{B}_0$ is specified by the position vector $\boldsymbol{X}$. In the deformed configuration $\mathcal{B}_t$, the points are at position vector $\boldsymbol{x}$ which is connected to $\boldsymbol{X}$ through the nonlinear deformation map $\boldsymbol{x} = \boldsymbol{\chi}(\boldsymbol{X})$. The deformation gradient $\boldsymbol{F}$ is defined as the gradient of the deformation map with respect to the material coordinates

$$\boldsymbol{F} = \operatorname{Grad} \boldsymbol{\chi}; \quad J = \det \boldsymbol{F}, \tag{1}$$

where J is the Jacobian determinant of the deformation gradient whose value should be greater than unity in order to avoid self penetration. Using the deformation gradient we can introduce the left and right Cauchy-Green tensors $\boldsymbol{b}$ and $\boldsymbol{C}$, respectively,

$$\boldsymbol{b} = \boldsymbol{F}\boldsymbol{F}^T, \quad \boldsymbol{C} = \boldsymbol{F}^T\boldsymbol{F}. \tag{2}$$

In the case of polymeric materials' modelling, the deformation gradient is usually decomposed into a volumetric (shape preserving but volume changing) and an isochoric (volume preserving but shape changing) part. Hence, the deformation gradient reads

$$\boldsymbol{F} = \boldsymbol{F}_{\text{vol}}\boldsymbol{F}_{\text{iso}} = \underbrace{J^{1/3}\boldsymbol{I}}_{\boldsymbol{F}_{\text{vol}}}\bar{\boldsymbol{F}}, \tag{3}$$

where $\boldsymbol{I}$ is the second order identity tensor and $\bar{\boldsymbol{F}} := \boldsymbol{F}_{\text{iso}}$ denotes the isochoric part of the deformation gradient $\boldsymbol{F}$.

2.2. Balance laws in electrostatics

2.2.1. Spatial configuration

In the case of vacuum, the electric displacement $\mathfrak{d}^{\varepsilon}$ is coupled to the electric field $\mathfrak{e}$ by the electric permittivity of vacuum ε_0

$$\mathfrak{d}^{\varepsilon} = \varepsilon_0 \mathfrak{e}, \quad \text{in } \mathcal{B}_t. \tag{4}$$

However, in the presence of a matter this equation is enhanced by the electric polarization $\mathbb{p}$. Hence the relationship among the electric displacement, the electric field and the polarization reads

$$\mathbb{d} = \varepsilon_0 \mathbb{e} + \mathbb{p} =: \mathbb{d}^{\varepsilon} + \mathbb{p}, \quad \text{in } \mathcal{B}_t. \tag{5}$$

If there are no free currents and free electric charges as in non-conducting materials, the electrical problem can be expressed by the corresponding Maxwell equations, which for the quasi-static case become

$$\text{curl } \mathbb{e} = \mathbf{0}, \quad \text{div } \mathbb{d} = 0 \quad \text{in } \mathcal{B}_t. \tag{6}$$

The curl of a vector will become zero when the vector is derived from a scalar potential. Hence equation $(6)_1$ is satisfied exactly if $\mathbb{e}$ derives from a scalar potential [74, 47, 78, 79], i.e.

$$\mathbb{e} = -\text{grad } \varphi. \tag{7}$$

In Eqn (7) grad φ is the gradient of the electric potential φ with respect to the spatial coordinates $\boldsymbol{x}$. The mechanical behavior is governed by the balance of linear momentum

$$\text{div } \boldsymbol{\sigma} + \boldsymbol{b}_t^{\text{pon}} + \boldsymbol{b}_t = \text{div } \boldsymbol{\sigma}^{\text{tot}} + \boldsymbol{b}_t = \mathbf{0}, \quad \text{in } \mathcal{B}_t, \tag{8}$$

where $\boldsymbol{b}_t$ is the mechanical body force, $\boldsymbol{b}_t^{\text{pon}}$ is the ponderomotive body force due to the field-matter interaction and $\boldsymbol{\sigma}^{\text{tot}}$ is the total Cauchy type symmetric stress tensor, cf. [17]. Furthermore, the total Cauchy type symmetric stress tensor $\boldsymbol{\sigma}^{\text{tot}}$ is decomposed into a non-symmetric mechanical Cauchy stress $\boldsymbol{\sigma}$ and a ponderomotive stress $\boldsymbol{\sigma}^{\text{pon}}$ [10] that satisfies

$$\text{div } \boldsymbol{\sigma}^{\text{pon}} = \boldsymbol{b}_t^{\text{pon}} = \text{grad } \mathbb{e} \cdot \mathbb{p}. \tag{9}$$

The ponderomotive stress can be decomposed into the non-symmetric polarization stress $\boldsymbol{\sigma}^{\text{pol}}$ [75] and the symmetric Maxwell stress $\boldsymbol{\sigma}^{\text{max}}$

$$\boldsymbol{\sigma}^{\text{pol}} = \mathbb{e} \otimes \mathbb{p}, \quad \boldsymbol{\sigma}^{\text{max}} = -\frac{1}{2}\varepsilon_0 [\mathbb{e} \cdot \mathbb{e}] \boldsymbol{i} + \varepsilon_0 \mathbb{e} \otimes \mathbb{e}, \tag{10}$$

where $\boldsymbol{i}$ is the second order identity tensor in the spatial configuration. In the absence of matter, i.e., in vacuum, the polarization $\mathbb{p}$, the Cauchy stress $\boldsymbol{\sigma}$ and the polarization stress $\boldsymbol{\sigma}^{\text{pol}}$ will disappear. However, the Maxwell stress and the electric displacement $\mathbb{d}^{\epsilon}$ exist and satisfy divergence free conditions

$$\text{div } \boldsymbol{\sigma}^{\text{max}} = \mathbf{0}, \qquad \text{div } \mathbb{d}^{\varepsilon} = 0. \tag{11}$$

The Dirichlet boundary conditions for the deformation map $\boldsymbol{\chi}$ are prescribed as

$$\boldsymbol{\chi} = \boldsymbol{\chi}^{\text{p}}, \quad \text{on } \partial\mathcal{B}_t^{\chi}. \tag{12}$$

When we consider prescribed mechanical tractions $\boldsymbol{t}_t^{\text{p}}$, the jump conditions regarding the total stress can be defined, with the help of the surface normal $\boldsymbol{n}$, on the surface of $\mathcal{B}_t$ [74]

$$[\![\boldsymbol{\sigma}^{\text{tot}}]\!] \cdot \boldsymbol{n} = -\boldsymbol{t}_t^{\text{p}}, \quad \text{on } \partial\mathcal{B}_t^{\text{t}}, \tag{13}$$

where $[\![\bullet]\!] = [\bullet^{\text{out}}] - [\bullet^{\text{in}}]$ represents the jump in a quantity across the boundary. The related jump conditions for the electrical quantities are defined as

$$[\![\mathbb{d}]\!] \cdot \boldsymbol{n} = \hat{\varrho}_t^f, \quad \text{on } \partial\mathcal{B}_t^{\varrho}, \quad \text{and} \quad [\![\mathbb{e}]\!] \times \boldsymbol{n} = 0, \quad \text{on } \partial\mathcal{B}_t \tag{14}$$

where $\hat{\varrho}_t^f$ is the density of free surface charges per undeformed area on the boundary [75].

2.2.2. Material configuration

Next we transform various electric quantities from the spatial configuration $\mathcal{B}_t$ to the undeformed configuration $\mathcal{B}_0$. Hence the electric field, the electric displacement field and the polarization vector read in the undeformed configuration as

$$\mathbb{E} = \boldsymbol{F}^T \mathbb{e}, \quad \mathbb{D} = J\boldsymbol{F}^{-1}\mathbb{d}, \quad \mathbb{P} = J\boldsymbol{F}^{-1}\mathbb{p}. \tag{15}$$

These will result in the Maxwell equations as

$$\text{Curl } \mathbb{E} = \boldsymbol{0}, \quad \text{Div } \mathbb{D} = 0, \tag{16}$$

where Curl and Div denote the corresponding differential operators with respect to the position vectors $\boldsymbol{X}$ in $\mathcal{B}_0$. Similar to the electric field in the spatial configuration, the first term in $(16)_1$ will be related to the scalar potential as

$$\mathbb{E} = -\text{Grad } \varphi, \quad \text{in } \mathcal{B}_0. \tag{17}$$

We introduce the electric displacement in the bulk as

$$\mathbb{D} = \varepsilon_0 J\boldsymbol{C}^{-1}\mathbb{E} + \mathbb{P} = \mathbb{D}^{\varepsilon} + \mathbb{P} \quad \text{in } \mathcal{B}_0. \tag{18}$$

Note that the referential format of the polarization is a pull-back operation of its spatial format (5). According to Dorfmann et al. [17], this definition is not unique as, for example, the definition of the polarization might alter. The total Cauchy stress $\boldsymbol{\sigma}^{\text{tot}}$ can be transformed into the material counterpart, the total Piola stress $\boldsymbol{P}^{\text{tot}}$

$$\boldsymbol{P}^{\text{tot}} = J\boldsymbol{\sigma}^{\text{tot}}\boldsymbol{F}^{-T}. \tag{19}$$

Similar to its spatial analogue, $\boldsymbol{P}^{\text{tot}}$ can be decomposed into the mechanical part $\boldsymbol{P}$ and the ponderomotive part $\boldsymbol{P}^{\text{pon}}$

$$\boldsymbol{P}^{\text{tot}} = \boldsymbol{P} + \boldsymbol{P}^{\text{pon}} = \boldsymbol{P} + \boldsymbol{P}^{\text{max}} + \boldsymbol{P}^{\text{pol}}, \tag{20}$$

where the polarization stress $\boldsymbol{P}^{\text{pol}}$ and the Maxwell stress $\boldsymbol{P}^{\text{max}}$ are expressed as

$$\boldsymbol{P}^{\text{pol}} = \mathbb{e} \otimes \mathbb{P}, \; \boldsymbol{P}^{\text{max}} = -\left[\frac{1}{2}\varepsilon_0 J\mathbb{E} \cdot [\boldsymbol{C}^{-1}\mathbb{E}]\right]\boldsymbol{F}^{-T} + \mathbb{e} \otimes \mathbb{D}^{\varepsilon}. \tag{21}$$

Note that the term $\frac{1}{2}\varepsilon_0 J\mathbb{E} \cdot [\boldsymbol{C}^{-1}\mathbb{E}]$ occuring in the Maxwell stress is nothing but the electrostatic energy density per unit volume in the material configuration. The balance of linear momentum (8) and the divergence free condition of the Maxwell stress (11) are transformed to

$$\text{Div } \boldsymbol{P}^{\text{tot}} + \boldsymbol{b}_0 = \boldsymbol{0} \quad \text{and} \quad \text{Div } \boldsymbol{P}^{\text{max}} = \boldsymbol{0}. \tag{22}$$

The corresponding boundary conditions in the material configuration read as

$$[\![\mathbb{D}]\!] \cdot \boldsymbol{N} = \varrho_0^f, \quad \text{on } \partial\mathcal{B}_0^\varrho, \quad \text{and} \quad [\![\boldsymbol{P}^{\text{tot}}]\!] \cdot \boldsymbol{N} = -\boldsymbol{t}_0^p, \quad \text{on } \partial\mathcal{B}_0^t, \tag{23}$$

where the relations $\hat{\varrho}_0^f dA = \hat{\varrho}_t^f da$ and $\boldsymbol{t}_0^p dA = \boldsymbol{t}_t^p da$ are used to transfer these quantities from the material configuration with area element dA to the spatial configuration with respective area element da.

3. Constitutive modelling

In this section, at first a technique to incorporate the dispersed chain contributions to the overall free energy function will be described. Thereafter, the averaging process to transfer the free energy contribution of the single chains from the microscopic level to the macroscopic continuum level will be elaborated. One of the key aspects of network theories is how to link up the deformation of a single chain in the microscopic level to the macroscopic isochoric deformation gradient, i.e., $\bar{\boldsymbol{F}}$. A mapping of the orientation vector $\boldsymbol{r}$, representing a single chain, by the isochoric deformation gradient of the continuum gives the isochoric stretch vector

$$\bar{\boldsymbol{t}} = \bar{\boldsymbol{F}}\boldsymbol{r}. \tag{24}$$

Then the macro-stretch $\bar{\lambda}$ of a material line element with the orientation $\bar{\boldsymbol{t}}$ in the current configuration is

$$\bar{\lambda} = |\bar{\boldsymbol{t}}| = \sqrt{\bar{\boldsymbol{t}} \cdot \bar{\boldsymbol{t}}} = \sqrt{\bar{\boldsymbol{F}}\boldsymbol{r} \cdot \bar{\boldsymbol{F}}\boldsymbol{r}} = \sqrt{\bar{\boldsymbol{C}} : [\boldsymbol{r} \otimes \boldsymbol{r}]}, \tag{25}$$

where $\bar{\boldsymbol{C}} = \bar{\boldsymbol{F}}^T \bar{\boldsymbol{F}}$ is the isochoric right Cauchy-Green strain tensor, see Miehe et al. [51, 52]. Similarly the electric field vector will be projected into the direction of the fibre $\boldsymbol{r}$ to obtain a fibre-oriented scalar electric field E as

$$E = \mathbb{E} \cdot \boldsymbol{r}, \tag{26}$$

where $\mathbb{E}$ is the electric field vector in the material configuration, see Thylander [71], Thylander et al. [72].

3.1. Energy decomposition

In particle-filled EAPs that are cured under an electric field, thanks to the experimental evidences in Fig (1), it can be assumed that the orientations of the chains within a family I (with $I = 1 \cdots N$) are distributed by a certain dispersion with respect to a mean referential (preferred) direction (say $\boldsymbol{a}_I$) over the surface of the unit-sphere $\mathbb{U}^2$. Such a family of chains constitutes a transversely isotropic contribution to the overall response of EAP composites. Hence the chain contributions, defined here as the anisotropic part, are added to the bulk part of the free energy. Following the analogy of the multiplicative decomposition of the deformation gradient in the case of polymeric materials in Eqn (3), a decoupled representation of the strain energy into a volumetric and an isochoric part is followed also in electro-elasticity as

$$\Psi = \Psi_{\text{vol}}(J) + \Psi_{\text{iso}}(\bar{\boldsymbol{C}}, \mathbb{E}; \boldsymbol{a}_1, \cdots, \boldsymbol{a}_N) = \Psi_{\text{vol}}(J) + \Psi_{\text{iso}}^{\text{isp}}(\bar{\boldsymbol{C}}, \mathbb{E}) + \Psi_{\text{iso}}^{\text{ani}}(\bar{\boldsymbol{C}}, \mathbb{E}, \boldsymbol{a}_1, \cdots, \boldsymbol{a}_N) \tag{27}$$

where $\Psi_{\text{vol}}(J)$ describes the change in the free energy due to volume changes and Ψ_{iso} describes the change in the free energy due to the isochoric deformation. Here the array of vectors, i.e., $\boldsymbol{a}_1, \cdots, \boldsymbol{a}_N$ represent the N families of fibres. The isochoric energy Ψ_{iso} is further decomposed into an isotropic part $\Psi_{\text{iso}}^{\text{isp}}$ and an anisotropic part $\Psi_{\text{iso}}^{\text{ani}}$, respectively.

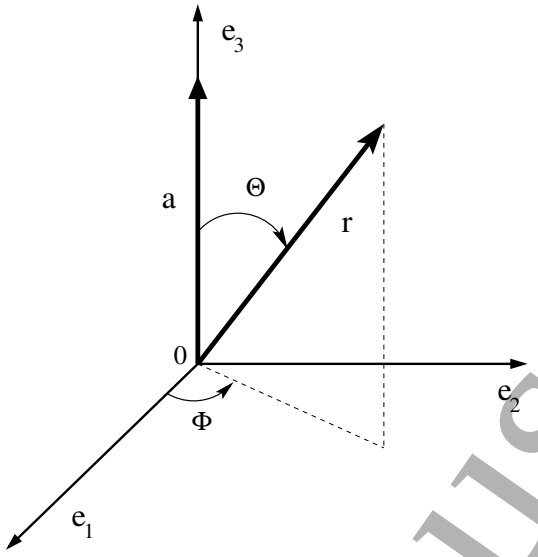

Figure 2: The orientation of a generic chain $\boldsymbol{r}$ in the three-dimensional space. Here, for the sake of presentation, the preferential unit vector $\boldsymbol{a}$ coincides with the Cartesian coordinate axis $\boldsymbol{e}_3$

3.2. Anisotropic energy contribution

Each chain orients in a direction designated by an arbitrary unit vector $\boldsymbol{r} \in \mathbb{U}^2$, $|\boldsymbol{r}| = 1$. The unit vector can be characterized by the use of Eulerian (spherical) angles, namely $\Theta \in [0, \pi]$ and $\Phi \in [0, 2\pi]$, cf. Fig (2). Therefore, the expression of the unit vector would be $\boldsymbol{r}(\Theta, \Phi) = \sin\Theta\cos\Phi\boldsymbol{e}_1 + \sin\Theta\sin\Phi\boldsymbol{e}_2 + \cos\Theta\boldsymbol{e}_3$, where $\{\boldsymbol{e}_i\}_{i=1,2,3}$ denote the axes of a rectangular Cartesian coordinate system. Note that each chain is counted twice by the above angles, i.e. for each $\boldsymbol{r}$, -$\boldsymbol{r}$ is also included. Similar to the chain orientation vector $\boldsymbol{r}$, the preferential (mean) vector $\boldsymbol{a}$ can also be expressed in terms of the Eulerian angles, i.e., $\boldsymbol{a}(\Theta^{\mathrm{m}}, \Phi^{\mathrm{m}}) = \sin\Theta^{\mathrm{m}}\cos\Phi^{\mathrm{m}}\boldsymbol{e}_1 + \sin\Theta^{\mathrm{m}}\sin\Phi^{\mathrm{m}}\boldsymbol{e}_2 + \cos\Theta^{\mathrm{m}}\boldsymbol{e}_3$, where $\Theta^{\mathrm{m}} \in [0, \pi]$ and $\Phi^{\mathrm{m}} \in [0, 2\pi]$.

The macroscopic energy density is derived from the microscopic contributions of single chain energy densities. Let us assume only one family I of chains that is symmetrically distributed along a preferred direction $\boldsymbol{a}_I \in \mathbb{U}^2$. If n number of chains exist per unit volume, then the anisotropic part of the macroscopic electromechanical coupled energy for this set of chains is defined as

$$\Psi_c^I(\bar{\boldsymbol{C}}, \mathbb{E}; \boldsymbol{a}_I) = \sum_{s=1}^{n} \rho(\boldsymbol{r}^s; \boldsymbol{a}_I)\psi_c^s(\bar{\boldsymbol{C}}, \mathbb{E}; \boldsymbol{r}^s) \tag{28}$$

where $\boldsymbol{r}^s \in \mathbb{U}^2$ are referential unit vectors associated with the direction of the s-th chain, and ψ_c^s is the microscopic strain energy of the s-th chain of family I according to the deformation in the direction of $\boldsymbol{r}^s$. In Eqn (28) $\rho(\boldsymbol{r}^s; \boldsymbol{a}_I)$ is a fibre probability distribution function which is explained in the next section. If we consider N preferred (mean) orientations $\boldsymbol{a}_1, \cdots, \boldsymbol{a}_N$ related to N families of chains, then the total isochoric chain energy will be

$$\Psi_{\mathrm{iso}}^{\mathrm{ani}}(\bar{\boldsymbol{C}}, \mathbb{E}; \boldsymbol{a}_1, \cdots, \boldsymbol{a}_N) = \sum_{I=1}^{N} \Psi_c^I(\bar{\boldsymbol{C}}, \mathbb{E}; \boldsymbol{a}_I) = \sum_{I=1}^{N}\sum_{s=1}^{n} \rho_I(\boldsymbol{r}^s)\psi_c^s(\bar{\lambda}_s, E_s), \tag{29}$$

where $E_s = \mathbb{E} \cdot \boldsymbol{r}^s$, $\bar{\lambda}_s = \sqrt{\bar{\boldsymbol{C}} : [\boldsymbol{r}^s \otimes \boldsymbol{r}^s]}$ and $\rho_I(\boldsymbol{r}^s) = \rho(\boldsymbol{r}^s; \boldsymbol{a}_I)$. For large n, the total isochoric chain energy function for a single family of fibres can be expressed as the weighted average of the n contributions, whereby the weight is the fibre probability distribution function $\rho_I = \rho_I(\boldsymbol{r}^s)$

$$\Psi_c^I(\bar{\boldsymbol{C}}, \mathbb{E}; \boldsymbol{a}_I) = \langle n \rho_I \psi_c(\bar{\lambda}, E) \rangle. \tag{30}$$

Here $\langle \bullet \rangle$ denotes a suited averaging operator for scalar quantities and $\bar{\lambda}$ (defined in Eqn (25)) is the macro stretch. In the following, we take an affine assumption for the micro to macro transformation. For the differences between affine and non-affine kinematics, see Miehe et al. [51]. An isotropic version of the averaging scheme in Eqn (30) proposed in the case of pure polymeric materials can be found in Miehe et al. [51, 52] while its anisotropic formulations in the case of biological tissue modelling is advocated in Alastrue et al. [1, 3]. The differential area element of the unit sphere $\mathbb{U}^2$ can be expressed in terms of the Eulerian angles as $dA = \sin\Theta d\Theta d\Phi$ while the surface integral yields the unit sphere's total area, i.e. $A_{\mathbb{U}^2} = \int_0^\Theta \int_0^\Phi dA = \int_0^\Theta \int_0^\Phi \sin\Theta d\Theta d\Phi = 4\pi$. Normalising the integral over the unit sphere, we obtain for the averaging operator

$$\langle n \rho_I \psi_c(\bar{\lambda}, E) \rangle = \frac{1}{4\pi} \int_{\mathbb{U}^2} n \rho_I \psi_c(\bar{\lambda}, E) dA. \tag{31}$$

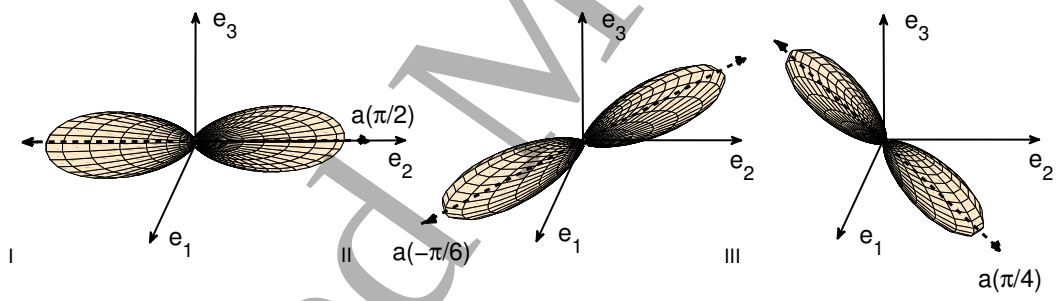

Figure 3: Illustrations of the fibre probability distribution function ρ for various orientations of the preferential unit vector $\boldsymbol{a}$; for a fixed value of $b = 3$ and $\Theta^{\mathrm{m}} = \pi/2$, (I) $\Phi^{\mathrm{m}} = \pi/2$, (II) $\Phi^{\mathrm{m}} = -\pi/6$, (III) $\Phi^{\mathrm{m}} = \pi/4$

3.3. von Mises distribution function

The symmetry condition for a single chain that is represented by its vector $\boldsymbol{r}$ has to be included into the PDF, i.e. $\rho(\boldsymbol{r}; \boldsymbol{a}) = \rho(-\boldsymbol{r}; \boldsymbol{a})$. Furthermore, it is assumed that the chains are rotational symmetrically distributed with respect to the preferred mean direction $\boldsymbol{a}$, i.e., $\rho(\boldsymbol{Q} \cdot \boldsymbol{r}; \boldsymbol{a}) = \rho(\boldsymbol{r}; \boldsymbol{a})\ \forall \boldsymbol{Q} \in \mathbb{Q}_+^3$ with rotation axis $\boldsymbol{a}$. We assume that the embedded chains are distributed transversely isotropic where the normalised π-periodic von Mises PDF can be applied that has the form

$$\rho(\chi) = 4\sqrt{\frac{b}{2\pi}}\frac{\exp(b[\cos(2\chi)+1])}{\operatorname{erfi}(\sqrt{2b})}. \tag{32}$$

Here the positive concentration parameter $b \in [0, \infty]$ represents a measure of *the degree of anisotropy*, $\operatorname{erfi}(x) = -i\,\operatorname{erf}(x)$ is the imaginary error function, and χ is the angle between unit vectors $\boldsymbol{r}$ and $\boldsymbol{a}$, i.e. the angle of a chain oriented by the vector $\boldsymbol{r}$ with the mean orientation of the chains denoted by the vector $\boldsymbol{a}$. The angle χ can be calculated by using the scalar product of $\boldsymbol{r}$ and $\boldsymbol{a}$, i.e.

$$\chi = \cos^{-1}(\boldsymbol{a} \cdot \boldsymbol{r}). \tag{33}$$

A three-dimensional presentation of the von Mises PDF is illustrated in the case of various orientations of the preferential vector $\boldsymbol{a}$ in Fig (3) while its significance with respect to different degree of dispersions b is presented in Fig (4) for $\boldsymbol{a} = \boldsymbol{e}_3$. It is clear from Fig (3) that the PDF is a symmetric function around the mean vector. Note that there are several other forms of symmetric and non-symmetric PDFs that can be utilised to capture chain orientation distribution, cf. Alasture et al. [2, 3].

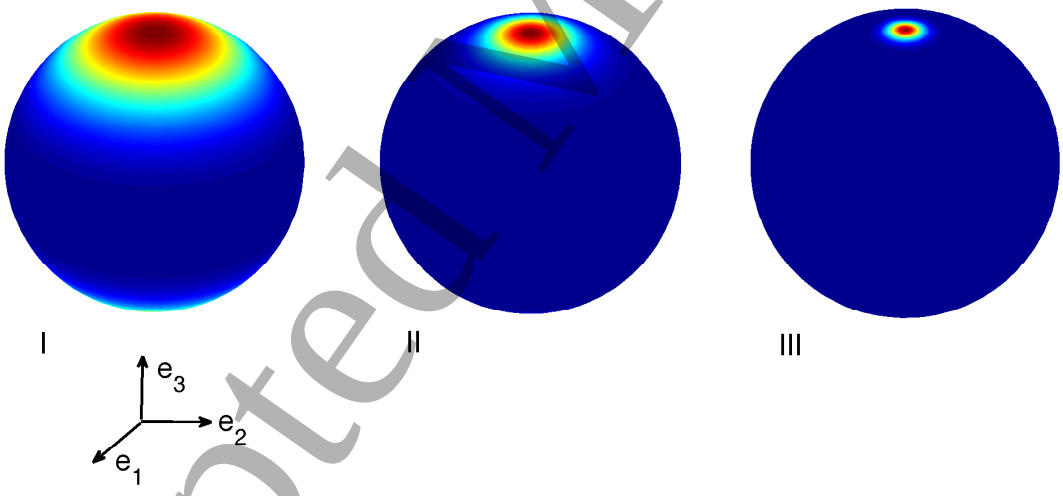

Figure 4: The three-dimensional representation of the von Mises probability distribution function (PDF) on the surface of a unit-sphere with respect to various *degree of dispersion* b. (I) $b = 0$, (II) $b = 3.0$, (III) $b = 20.0$. For the illustration purpose, the preferential unit vector $\boldsymbol{a}$ is considered in the vertical direction $\boldsymbol{e}_3$. The colour corresponds to the magnitude of the PDF ρ

3.4. Discretization over the micro-sphere

Concerning the averaging of the quantities in Eqn (31) over the unit sphere, numerical techniques, similar to numerical quadrature in the finite element method, can be used. By using prescribed direction vectors

and non-negative weighting factors the exact continuous integration can be approximated. Hence the discrete form of the continuous fibre probability distribution function over the unit sphere, by assuming nid orientation vectors $\{\boldsymbol{r}^s\}_{s=1,\cdots,\text{nid}}$ along with nid weighting factors $\{w^s\}_{s=1,\cdots,\text{nid}}$, can be expressed as

$$\langle(\bullet)\rangle = \frac{1}{4\pi}\int_{\mathbb{U}^2}(\bullet)dA \approx \sum_{s=1}^{\text{nid}}(\bullet)^s w^s. \tag{34}$$

Such a discrete integration scheme can be interpreted as $(\bullet)^s$ is the value of $(\bullet)$ in the direction of $\boldsymbol{r}^s$ scaled with non-negative integration weights w^s that hold the condition $\sum_{s=1}^{\text{nid}} w^s = 1$ to ensure the exact integration of constant functions, cf. Verron [73]. There are, according to Bazant & Oh [6], two more constraints that need to be satisfied

$$\langle\boldsymbol{r}\rangle \approx \sum_{s=1}^{\text{nid}} w^s\boldsymbol{r}^s = \boldsymbol{0}, \quad \text{and} \quad \langle\boldsymbol{r}\otimes\boldsymbol{r}\rangle \approx \sum_{s=1}^{\text{nid}} w^s\boldsymbol{r}^s\otimes\boldsymbol{r}^s = \frac{1}{3}\boldsymbol{I}. \tag{35}$$

The latter constraint ensures the stress-free state of the macro-continuum in the reference configuration. Moreover, both conditions preserve the isotropy for a constant value of the PDF, i.e. $\rho = \text{const}$, see, Miehe et al. [51], Alastrue et al. [2]. One of the key advantages of the micro-sphere-based framework is that any one-dimensional constitutive equation, that is suggested by experimental evidences, can straightforwardly be transferred to the general three-dimensional form. Despite the high computational costs, thanks to the simple formulation where complicated tensorial formulations are absent, the micro-sphere based AI-models obtain popularity in many areas of constitutive modelling, see for details, Etse et al. [25], Kuhl et al. [41], Miehe et al. [51], Alastrue et al. [1, 2], Ehret et al. [24].

3.5. Stress calculations

The concept of a total energy function is common in the area of electro-and magneto-elasticity as demonstrated by Dorfmann & Ogden [17, 18]. Thereby the total energy Ω can be written as

$$\Omega(\boldsymbol{F},\mathbb{E}) = \Psi(\boldsymbol{F},\mathbb{E}) + E_0(\boldsymbol{F},\mathbb{E}), \tag{36}$$

where $E_0 = -\frac{1}{2}\varepsilon_0 J\mathbb{E}\cdot[\boldsymbol{C}^{-1}\mathbb{E}]$ denotes the electrostatic energy density per unit volume in the material configuration. As is demonstrated in [74] the total energy changes the dissipation inequality to

$$\boldsymbol{P}^{\text{tot}} : \dot{\boldsymbol{F}} - \dot{\Omega} - \mathbb{D}\cdot\dot{\mathbb{E}} \overset{!}{\geq} 0, \tag{37}$$

for all possible thermodynamic admissible processes. Therefore, the constitutive relations modify to

$$\boldsymbol{P}^{\text{tot}} = \frac{\partial\Omega}{\partial\boldsymbol{F}}, \quad \text{with} \quad \boldsymbol{P}^{\text{max}} = \frac{\partial E_0}{\partial\boldsymbol{F}}, \quad \mathbb{D} = -\frac{\partial\Omega}{\partial\mathbb{E}}. \tag{38}$$

Moreover, in many cases, expressions for the total stress have to be written either in terms of the total Cauchy stress or in terms of the total Piola-Kirchhoff stress tensor, i.e.

$$\boldsymbol{\sigma}^{\text{tot}} = J^{-1}\frac{\partial\Omega}{\partial\boldsymbol{F}}\boldsymbol{F}^T, \quad \boldsymbol{S}^{\text{tot}} = 2\frac{\partial\Omega}{\partial\boldsymbol{C}}. \tag{39}$$

In the case of rubber-like materials' modelling where the additive decomposition into volumetric and iso-

choric energy contributions is assumed, i.e., with the help of Eqn (27), the total energy function becomes

$$\Omega(\boldsymbol{F},\mathbb{E}) = \Psi(\boldsymbol{F},\mathbb{E}) + E_0(\boldsymbol{F},\mathbb{E}) = \Psi_{\text{vol}}(J) + \Psi^{\text{isp}}_{\text{iso}}(\bar{\boldsymbol{C}},\mathbb{E}) + \Psi^{\text{ani}}_{\text{iso}}(\bar{\boldsymbol{C}},\mathbb{E};\boldsymbol{a}_1,\cdots,\boldsymbol{a}_N) + E_0(\boldsymbol{F},\mathbb{E}). \quad (40)$$

The total Piola-Kirchhoff stress for a nearly incompressible electro-active coupled polymeric material can be calculated as

$$\begin{aligned}
\boldsymbol{S}^{\text{tot}} &= 2\frac{\partial \Psi_{\text{iso}}}{\partial \boldsymbol{C}} + 2\frac{\partial \Psi_{\text{vol}}}{\partial \boldsymbol{C}} + 2\frac{\partial E_0}{\partial \boldsymbol{C}} \\
&= 2\frac{\partial \Psi_{\text{iso}}}{\partial \boldsymbol{C}} + Jp\,\boldsymbol{C}^{-1} + \varepsilon_0 J\left[[\boldsymbol{C}^{-1}\cdot\mathbb{E}]\otimes[\mathbb{E}\cdot\boldsymbol{C}^{-1}] - \frac{1}{2}[\mathbb{E}\cdot\boldsymbol{C}^{-1}\cdot\mathbb{E}]\boldsymbol{C}^{-1}\right] \\
&= J^{-\frac{2}{3}}\mathbb{P} : 2\frac{\partial \Psi_{\text{iso}}}{\partial \bar{\boldsymbol{C}}} + Jp\,\boldsymbol{C}^{-1} + \varepsilon_0 J\left[[\boldsymbol{C}^{-1}\cdot\mathbb{E}]\otimes[\mathbb{E}\cdot\boldsymbol{C}^{-1}] - \frac{1}{2}[\mathbb{E}\cdot\boldsymbol{C}^{-1}\cdot\mathbb{E}]\boldsymbol{C}^{-1}\right] \\
&= J^{-\frac{2}{3}}\mathbb{P} : \bar{\boldsymbol{S}} + Jp\,\boldsymbol{C}^{-1} + \varepsilon_0 J\left[[\boldsymbol{C}^{-1}\cdot\mathbb{E}]\otimes[\mathbb{E}\cdot\boldsymbol{C}^{-1}] - \frac{1}{2}[\mathbb{E}\cdot\boldsymbol{C}^{-1}\cdot\mathbb{E}]\boldsymbol{C}^{-1}\right]
\end{aligned} \quad (41)$$

where $\mathbb{P} = \mathbb{I} - \frac{1}{3}\boldsymbol{C}^{-1}\otimes\boldsymbol{C}, \mathbb{I} = \delta_{ik}\delta_{jl}$, $\bar{\boldsymbol{C}} = J^{-2/3}\boldsymbol{C}$ and the hydrostatic pressure $p = \partial\Psi_{\text{vol}}(J)/\partial J$ has been introduced. In the case of incompressibility, $J = 1$ and p serves as a Lagrange multiplier to satisfy this kinematic constraint on the deformation field. Note that there are several proposals for the volumetric part of the energy function Ψ_{vol}, see Steinmann et al. [62], Hossain & Steinmann [32]. Now we can go back to the isochoric part of the energy function as

$$\begin{aligned}
\Psi_{\text{iso}}(\bar{\boldsymbol{C}},\mathbb{E};\boldsymbol{a}_1,\cdots,\boldsymbol{a}_N) &= \Psi^{\text{isp}}_{\text{iso}}(\bar{\boldsymbol{C}},\mathbb{E}) + \Psi^{\text{ani}}_{\text{iso}}(\bar{\boldsymbol{C}},\mathbb{E};\boldsymbol{a}_1,\cdots,\boldsymbol{a}_N) \\
&= \Psi^{\text{isp}}_{\text{iso}}(\bar{I}_1,\cdots\bar{I}_6) + \Psi^{\text{ani}}_{\text{iso}}(\bar{\boldsymbol{C}},\mathbb{E};\boldsymbol{a}_1,\cdots,\boldsymbol{a}_N)
\end{aligned} \quad (42)$$

where for isotropy, the energy function $\Psi^{\text{isp}}_{\text{iso}}$ depends on the electro-mechanical coupled invariants, i.e. $\bar{I}_1$ to $\bar{I}_6$. Thereby the electro-mechanical coupled invariants $(\bar{I}_1,\bar{I}_2,\bar{I}_4,\bar{I}_5,\bar{I}_6)$ are defined as a combination of the isochoric right Cauchy-Green tensor $\bar{\boldsymbol{C}}$ and the electric field $\mathbb{E}$ in the material configuration

$$\begin{aligned}
&\bar{I}_1 = \text{tr}(\bar{\boldsymbol{C}}); && \bar{I}_2 = \frac{1}{2}\Big[[\text{tr}(\bar{\boldsymbol{C}})]^2 - \text{tr}(\bar{\boldsymbol{C}}^2)\Big]; && \bar{I}_3 = \det(\bar{\boldsymbol{F}}); \\
&\bar{I}_4 = [\mathbb{E}\otimes\mathbb{E}] : \boldsymbol{I}; && \bar{I}_5 = [\mathbb{E}\otimes\mathbb{E}] : \bar{\boldsymbol{C}}^{-1}; && \bar{I}_6 = [\mathbb{E}\otimes\mathbb{E}] : \bar{\boldsymbol{C}}^{-2}.
\end{aligned} \quad (43)$$

Now the isochoric part of the Piola-Kirchhoff stress tensors can be calculated as

$$\begin{aligned}
\bar{\boldsymbol{S}} &= 2\frac{\partial \Psi_{\text{iso}}}{\partial \bar{\boldsymbol{C}}} \\
&= 2\frac{\partial \Psi^{\text{isp}}_{\text{iso}}}{\partial \bar{\boldsymbol{C}}} + 2\frac{\partial \Psi^{\text{ani}}_{\text{iso}}}{\partial \bar{\boldsymbol{C}}} \\
&= 2\left[\frac{\partial \Psi^{\text{isp}}_{\text{iso}}}{\partial \bar{I}_1}\frac{\partial \bar{I}_1}{\partial \bar{\boldsymbol{C}}} + \frac{\partial \Psi^{\text{isp}}_{\text{iso}}}{\partial \bar{I}_2}\frac{\partial \bar{I}_2}{\partial \bar{\boldsymbol{C}}} + \frac{\partial \Psi^{\text{isp}}_{\text{iso}}}{\partial \bar{I}_5}\frac{\partial \bar{I}_5}{\partial \bar{\boldsymbol{C}}} + \frac{\partial \Psi^{\text{isp}}_{\text{iso}}}{\partial \bar{I}_6}\frac{\partial \bar{I}_6}{\partial \bar{\boldsymbol{C}}}\right] + 2\frac{\partial \Psi^{\text{ani}}_{\text{iso}}}{\partial \bar{\boldsymbol{C}}} \\
&= 2\Psi^{\text{isp}}_{\text{iso},1}\boldsymbol{I} + 2\Psi^{\text{isp}}_{\text{iso},2}[\bar{I}_1\boldsymbol{I} - \bar{\boldsymbol{C}}] - 2\Psi^{\text{isp}}_{\text{iso},5}\Big[\bar{\boldsymbol{C}}^{-T}\cdot[\mathbb{E}\otimes\mathbb{E}]\cdot\bar{\boldsymbol{C}}^{-1}\Big] \\
&\quad - 2\Psi^{\text{isp}}_{\text{iso},6}\Big[[\bar{\boldsymbol{C}}^{-1}\cdot\bar{\boldsymbol{C}}^{-T}]\mathbb{E}\otimes[\bar{\boldsymbol{C}}^{-1}\mathbb{E}] - [\bar{\boldsymbol{C}}^{-1}\mathbb{E}]\otimes[\bar{\boldsymbol{C}}^{-1}\cdot\bar{\boldsymbol{C}}^{-T}]\mathbb{E}\Big] + 2\frac{\partial \Psi^{\text{ani}}_{\text{iso}}}{\partial \bar{\boldsymbol{C}}}
\end{aligned} \quad (44)$$

where derivatives of the isochoric energy function with respect to the coupled invariants are denoted as $\frac{\partial \Psi^{\text{isp}}_{\text{iso}}}{\partial \bar{I}_i} =: \Psi^{\text{isp}}_{\text{iso},i}$. Once we identify an appropriate microscopic strain energy for a single chain ψ_c, whereby we shall here assume only one family of chains, the anisotropic part of the isochoric stress tensor will be as follows

$$\bar{\boldsymbol{S}}^{\text{ani}} = 2\frac{\partial \Psi^{\text{ani}}_{\text{iso}}}{\partial \bar{\boldsymbol{C}}} \approx \sum_{s=1}^{\text{nid}} 2\rho^s \frac{\partial \psi^s_c}{\partial \bar{\lambda}^2_s}\frac{\partial \bar{\lambda}^2_s}{\partial \bar{\boldsymbol{C}}} w^s = \sum_{s=1}^{\text{nid}} 2\rho^s \frac{1}{2}\frac{1}{\bar{\lambda}_s}\frac{\partial \psi^s_c}{\partial \bar{\lambda}_s}\boldsymbol{r}^s \otimes \boldsymbol{r}^s w^s = \sum_{s=1}^{\text{nid}} \rho^s [\bar{\lambda}]^{-1}_s \frac{\partial \psi^s_c}{\partial \bar{\lambda}_s}\boldsymbol{r}^s \otimes \boldsymbol{r}^s w^s, \tag{45}$$

where $\rho^s = \rho(\boldsymbol{r}^s; \boldsymbol{a})$. Similar to the total coupled stress tensor, the total electric displacement will be the combination of isotropic and anisotropic parts as

$$\mathbb{D} = -\frac{\partial \Omega}{\partial \mathbb{E}} = \mathbb{D}^{\text{iso}} + \mathbb{D}^{\text{ani}} \tag{46}$$

where

$$\mathbb{D}^{\text{ani}} = -\frac{\partial \Psi^{\text{ani}}}{\partial \mathbb{E}} \approx -\sum_{s=1}^{\text{nid}} \rho^s \frac{\partial \psi^s_c}{\partial E_s}\boldsymbol{r}^s w^s. \tag{47}$$

4. Benchmark examples

In this section, we identify relevant material parameters from isotropic EAPs. Using the identified parameters, the capability of the proposed dispersed anisotropic electro-elastic modelling framework is demonstrated by solving a non-homogeneous boundary value problem. In order to obtain the complete expression for the energy function in Eqn (40), appropriate choices for the isotropic energy function $\Psi^{\text{isp}}_{\text{iso}}$ as well as for the anisotropic energy function $\Psi^{\text{ani}}_{\text{iso}}$ need to be determined. The Neo-Hookean type electro-mechanically coupled strain energy function is often used in electro-elasticity. Hence, as a starting point, we assume a Neo-Hookean-like material as in [79] depending on the purely mechanical invariant $\bar{I}_1$, the electrical invariant $\bar{I}_4$ and the coupled invariant $\bar{I}_5$ where the shear modulus μ depends on the electric field via $\bar{I}_4$. Other advanced forms of energy functions for rubber-like materials can be coupled with the electric part of the energy to improve the modelling, cf. [32, 33, 62]. A Neo-Hookean coupled isotropic free energy function is thus

$$\Psi^{\text{isp}}_{\text{iso}}(\bar{\boldsymbol{C}}, \mathbb{E}) = \mu(\bar{I}_4)\left[\bar{I}_1 - 3\right] + c_e\bar{I}_4 + c_m\bar{I}_5, \tag{48}$$

where c_e and c_m are called electrostrictive coupling coefficients. Mimicking the isotropic part of the macroscopic energy appearing in Eqn (48), a Neo-Hookean type free energy function for a single chain fibre can be chosen. In order to facilitate a closed-form solution of a non-homogeneous boundary value problem discussed in the next section, we choose the free energy function for a single chain from Thylander et al. [71]. They used this energy function for micro-sphere based isotropic electro-elasticity. Note that there are several other proposals for free energy functions for a single chain fibre in the case of biological tissue modelling, e.g., Fung-type model, Worm-like chain model etc, see Alastrue et al.[1] for more details. After performing the averaging operation on the unit sphere including scaling by the von Mises PDF ρ for a single family of

fibres, we obtain the macroscopic form of the anisotropic energy function as

$$\Psi^{\text{ani}}_{\text{iso}}(\bar{\boldsymbol{C}}, \mathbb{E}; \boldsymbol{a}) \approx \sum_{s=1}^{\text{nid}} \rho^s \, \psi^s_c \, w^s = \sum_{s=1}^{\text{nid}} \rho^s \underbrace{\left[\frac{1}{2}\tilde{\mu}[\bar{\lambda}_s^2 - 1] + c_1 \bar{\lambda}_s^2 E_s^2 + c_2 E_s^2\right]}_{\psi^s_c} w^s \tag{49}$$

where $\tilde{\mu}$, c_1 and c_2 are the chain shear modulus and the coupling parameters, respectively, in the micro-sphere energy function ψ^s_c. Finally, after combining the isotropic coupled function in (48) and the anisotropic coupled function in (49), a complete form of the energy function becomes

$$\Psi_{\text{iso}}(\bar{\boldsymbol{C}}, \mathbb{E}; \boldsymbol{a}) = \mu(\bar{I}_4)\left[\bar{I}_1 - 3\right] + c_e \bar{I}_4 + c_m \bar{I}_5 + \sum_{s=1}^{\text{nid}} \rho^s \left[\frac{1}{2}\tilde{\mu}[\bar{\lambda}_s^2 - 1] + c_1 \bar{\lambda}_s^2 E_s^2 + c_2 E_s^2\right] w^s. \tag{50}$$

Exploring the constraint conditions described in Eqns (35), Thylander [71], Thylander et al. [72] established that there are excellent correlations between parameters appearing in the macroscopic bulk energy and the micro-sphere chain energy, i.e. $\tilde{\mu} = 3\mu, c_1 = 3c_m, c_2 = 3c_e$. Therefore, at this stage, all parts of the energy function expressed in Eqn (40) are obtained. Using the definition of the Piola-Kirchhoff stress tensor as in Eqn (44), the isochoric part of the total stress, that also contains the chain contribution, will be as follows

$$\bar{\boldsymbol{S}} = 2\frac{\partial \Psi_{\text{iso}}}{\partial \bar{\boldsymbol{C}}} = \mu \boldsymbol{I} + 2c_m \mathbb{I}_{\bar{\boldsymbol{C}}^{-1}} : [\mathbb{E} \otimes \mathbb{E}] + \sum_{s=1}^{\text{nid}} \rho^s [\bar{\lambda}]_s^{-1} \frac{\partial \psi^s_c}{\partial \bar{\lambda}_s} \boldsymbol{r}^s \otimes \boldsymbol{r}^s w^s, \tag{51}$$

where $\mathbb{I}^{\text{ABCD}}_{\bar{\boldsymbol{C}}^{-1}} = -\frac{1}{2}\left[\bar{C}^{-1}_{\text{AC}}\bar{C}^{-1}_{\text{BD}} + \bar{C}^{-1}_{\text{AD}}\bar{C}^{-1}_{\text{BC}}\right]$. The electric displacement with regard to the reference configuration is derived as

$$\mathbb{D} = \varepsilon_0 J \boldsymbol{C}^{-1} \cdot \mathbb{E} - 2c_e \mathbb{E} - 2c_m \bar{\boldsymbol{C}} \cdot \mathbb{E} - \sum_{s=1}^{\text{nid}} \rho^s \frac{\partial \psi^s_c}{\partial E_s} \boldsymbol{r}^s w^s. \tag{52}$$

Due to the small value of the vacuum permittivity, the free space term in the total energy formulation (40) will be neglected in the sequel as in [78, 45], i.e. $\Omega(\boldsymbol{F}, \mathbb{E}, \boldsymbol{a}) \approx \Psi(\boldsymbol{F}, \mathbb{E}, \boldsymbol{a})$ is assumed in the subsequent calculations. Moreover, in all numerical examples presented in the following sections, we adopt the frequently-used assumption of incompressibility in the case of rubber-like material modelling.

4.1. Parameter identification from homogeneous isotropic EAPs

At first we would like to identify relevant material parameters appearing in the modelling frameworks using existing experimental data. There are several experimental data available in the literature, e.g., Carpi et al. [13], Diaconu et al. [22], Kollosche et al. [43]. However, all of the existing experiments, to the best of the authors' knowledge, are performed on isotropic polymeric materials under electro-mechanical coupled loads. None of the data is obtained from chain-dispersed filled EAPs. We have systematically illustrated in Eqns (40-45) that the proposed modelling framework is based on two parts of the energy function, i.e. isotropic and anisotropic parts where the latter is scaled by a dispersion parameter b to capture the degree of concentration of the dispersed polymer chains. To identify mechanical material parameters as well as electro-mechanical coupled parameters, we select the data obtained by Carpi et al. [13]. Carpi and co-

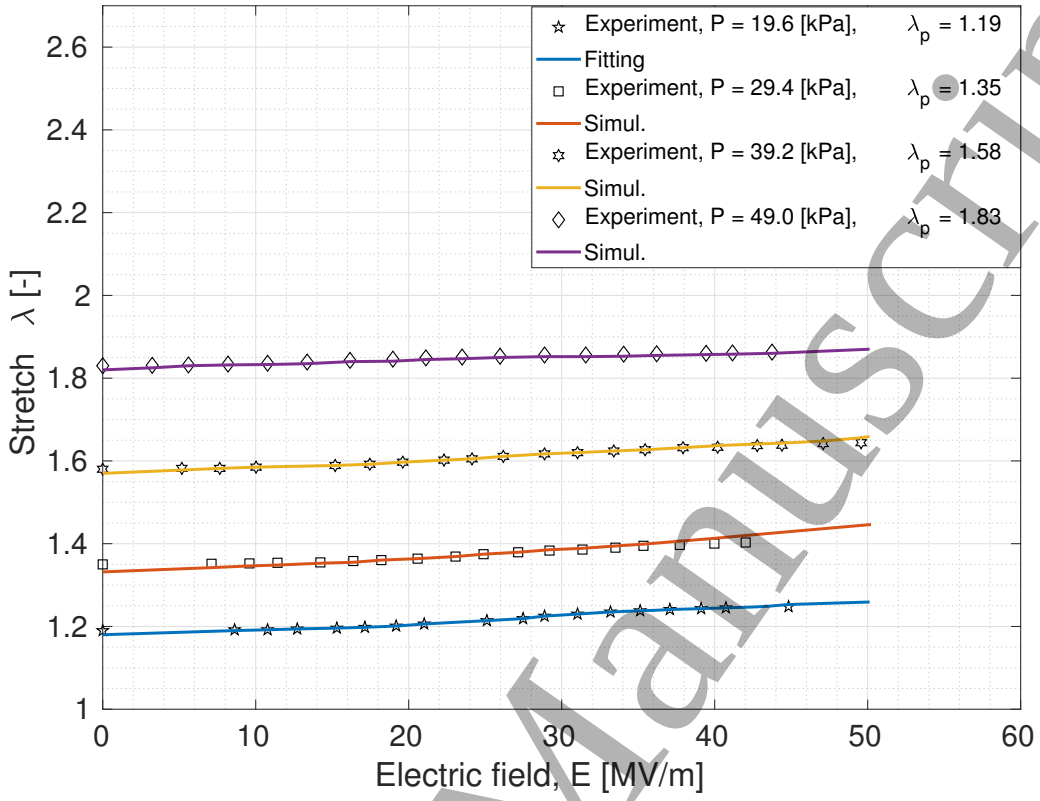

Figure 5: Parameter identifications and model predictions for the experimental data by Carpi et al. [13]. The specimen was 50 micro-meter thick acrylic polymeric film VHB that was pre-stretched in the longitudinal direction: longitudinal stretch (λ) versus the electric field (E) applied in the thickness direction

workers conducted experiments on a rectangular specimen made of 50 micro-meter thick acrylic polymeric film, commercially known as VHB (very high bond) F9460PC. For electric actuations, specimens were coated by different electrode materials where samples were subjected first to different pre-stresses P in the vertical (longitudinal) direction. After sufficient pre-stressing, specimens were thin enough to be activated for significant actuations. Then various amount of electric fields were applied in the thickness direction. The dimensions of the specimen were 3cm (longitudinal) x 2cm (transverse). Despite the application of the electric field within a very short amount of time (2 seconds) in the thickness direction, voltage induces a change of the stretch in the longitudinal direction. They conducted experiments with four different compliant electrodes, e.g. electrolyte solution, carbon grease, graphite spray and graphite powder. However, we only take the data produced by graphite powder electrode. For the geometry and boundary conditions mentioned above, for the modelling purpose, specimens are idealised under uniaxial tensions with electro-mechanical coupled loads.

To validate our model against the data that are for isotropic polymeric materials, we assume that the (imaginary) particles are homogeneously distributed in the matrix. Hence the concentration parameter b is set to its minimum value, i.e. $b \to 0$. At first, we identify only mechanical parameters, i.e. μ and $\tilde{\mu}$ by setting $E = 0$ in the stress expression derived from Eqn (50). In this case, different pre-stresses

$P = [19.6, 29.4, 39.2, 49.0]$kPa are plotted against the pre-stretches $\lambda_p = [1.19, 1.35, 1.58, 1.83]$. By fitting the stress equation obtained by the energy function in Eqn (50), the mechanical parameters μ (hence $\tilde{\mu}$ as $\tilde{\mu} = 3\mu$) is obtained, i.e. $\mu = 0.81$kPa. Now, we fit the electro-mechanical coupled model assuming that the (imaginary) particles are homogeneously distributed in the matrix characterized by a minimum value of b. In Fig (5) the change of the stretch of the film in the longitudinal direction is plotted against the electric field in the thickness direction for various values of the pre-stresses P. By fitting the model with the first set of data starting with the pre-stretch $\lambda_p = 1.19$, we obtain the coupled parameters $c_m = 3.25 \cdot 10^{-14} \frac{F}{m}$ (hence c_1 as $c_1 = 3c_m$). During the identification of the coupled parameters, the mechanical parameters are kept frozen. Once all relevant parameters are identified, the change of the stretch in the longitudinal direction is simulated for other three sets of data. In Fig (5) one can observe a very good agreement between the experimental data and model predictions.

4.2. Non-homogeneous deformation

For non-homogeneous deformations, the extension and inflation of an incompressible cylindrical tube with a cylindrical symmetry has been explored in various areas ranging from nonlinear elasticity to nonlinear electro-and magneto-mechanical coupling problems, cf. [17, 18, 19, 20, 53]. Bustamante [8, 9] has demonstrated this example both for electro-mechanical and magneto-mechanical cases with transverse isotropy while Mehnert et al. [45, 46] extended it towards thermo-electro-mechanical and thermo-magneto-mechanical couplings. Therefore, we adopt this example to reproduce some results by the newly proposed constitutive framework that can quantitatively be matched with results available in the literature. Moreover, this particular problem will show how the degree of dispersion of polymer chains influences the actuation behaviours. Due to the cylindrical geometry, it is reasonable to work in cylindrical coordinates. Expressing the divergence of the electric displacement div $\mathbb{d} = 0$ in cylindrical coordinates in the actual configuration, we find

$$\frac{1}{r}\mathbb{d}_r + \frac{\partial \mathbb{d}_r}{\partial r} + \frac{1}{r}\frac{\partial \mathbb{d}_\phi}{\partial \phi} + \frac{\partial \mathbb{d}_z}{\partial z} = 0, \tag{53}$$

and for the curl of the electric field curl $\mathbb{e} = \mathbf{0}$

$$\frac{1}{r}\frac{\partial \mathbb{e}_z}{\partial \phi} - \frac{\partial \mathbb{e}_\phi}{\partial z} = 0; \quad \frac{\partial \mathbb{e}_r}{\partial z} - \frac{\partial \mathbb{e}_z}{\partial r} = 0; \quad \frac{1}{r}\frac{\partial (r\mathbb{e}_\phi)}{\partial r} - \frac{1}{r}\frac{\partial \mathbb{e}_r}{\partial \phi} = 0, \tag{54}$$

where the components of the electric field $\mathbb{e}$ and the electric displacement $\mathbb{d}$ are expressed as $(\mathbb{e}_r, \mathbb{e}_\phi, \mathbb{e}_z)$ and $(\mathbb{d}_r, \mathbb{d}_\phi, \mathbb{d}_z)$, respectively. The cylindrical symmetry of the tube geometry results in invariance of the field quantity with respect to ϕ and z, i.e. $\frac{\partial(\bullet)}{\partial \phi} = \frac{\partial(\bullet)}{\partial z} = 0$. Hence, equations (53) and (54) reduce to

$$r\mathbb{d}_r = \text{constant}; \quad r\mathbb{e}_\phi = \text{constant}; \quad \mathbb{e}_z = \text{constant}. \tag{55}$$

The divergence of the total Cauchy stress tensor in cylindrical coordinates in a cylindrically symmetric stress state is expressed as

$$\text{div}\, \boldsymbol{\sigma}^{\text{tot}} = \left[\frac{\partial \sigma^{\text{tot}}_{rr}}{\partial r} + \frac{\sigma^{\text{tot}}_{rr} - \sigma^{\text{tot}}_{\phi\phi}}{r}\right] \boldsymbol{e}_r + \left[\frac{\partial \sigma^{\text{tot}}_{r\phi}}{\partial r} + \frac{2\sigma^{\text{tot}}_{r\phi}}{r}\right] \boldsymbol{e}_\phi + \left[\frac{\partial \sigma^{\text{tot}}_{rz}}{\partial r} + \frac{\sigma^{\text{tot}}_{rz}}{r}\right] \boldsymbol{e}_z. \tag{56}$$

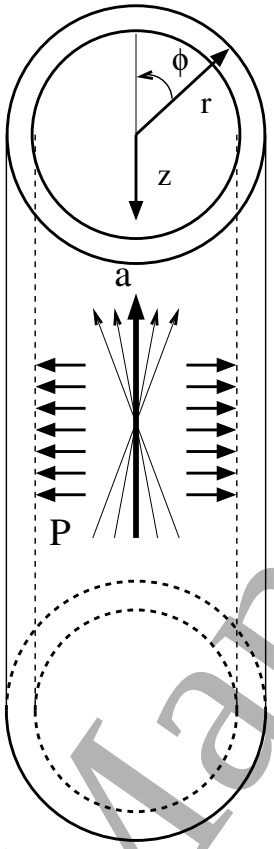

Figure 6: A cylindrical tube being inflated under an internal pressure P where the preferred (mean) direction $\boldsymbol{a}$ is aligned in the vertical axis. The chains are dispersed symmetrically along the preferred axis $\boldsymbol{a}$

4.2.1. Extension and inflation of a tube

We consider a thick-walled tube in cylindrical coordinates, see Fig (6). The geometry in the spatial configuration is described by

$$a_i \leq r \leq a_e; \quad 0 \leq \phi \leq 2\pi; \quad 0 \leq z \leq l, \tag{57}$$

where a_i and a_e denote the inner and outer radii in the deformed configuration, respectively. The tube geometry can be described in the material configuration by

$$A_i \leq R \leq A_e; \quad 0 \leq \Phi \leq 2\pi; \quad 0 \leq Z \leq L, \tag{58}$$

where A_i and A_e denote the inner and outer radii in the undeformed configuration, respectively. The deformation in the tube is activated under a combination of an axial extension and a radial expansion. Hence due to the combined action of inflation and extension, the transformation from the undeformed to the deformed configuration is described by

$$r^2 = \lambda_z^{-1}\Big[R^2 - A_i^2\Big] + a_i^2, \quad \phi = \Phi, \quad z = \lambda_z Z, \tag{59}$$

where λ_z is the uniform axial stretch. In formulating the first part of the above relation, the incompressibility assumption is applied, i.e. $\lambda_1\lambda_2\lambda_3 \equiv 1$. Note that for the problem under consideration, the deformation gradient has only entries on the main diagonal. In cylindrical coordinates the radial, circumferential/azimuthal and axial entries read

$$\lambda_r = [\lambda\lambda_z]^{-1}; \quad \lambda_\phi = \frac{r}{R} = \lambda; \quad \lambda_z. \tag{60}$$

Due to the deformation gradient presented above, the electric field vector in the spatial configuration takes the form

$$\mathbb{e}_r = \lambda\lambda_z\mathbb{E}_R, \mathbb{e}_\phi = \lambda^{-1}\mathbb{E}_\Phi, \mathbb{e}_z = \lambda_z^{-1}\mathbb{E}_Z. \tag{61}$$

For the inflation and extension of the tube, the divergence of the total stress $\mathrm{div}\boldsymbol{\sigma}^{\mathrm{tot}} = \mathbf{0}$ can be formulated from Eqn (56) as

$$\frac{\partial\sigma_{rr}^{\mathrm{tot}}}{\partial r} + \frac{\sigma_{rr}^{\mathrm{tot}} - \sigma_{\phi\phi}^{\mathrm{tot}}}{r} = 0, \tag{62a}$$

$$\frac{\partial\sigma_{r\phi}^{\mathrm{tot}}}{\partial r} + \frac{2\sigma_{r\phi}^{\mathrm{tot}}}{r} = 0 \tag{62b}$$

$$\frac{\partial\sigma_{rz}^{\mathrm{tot}}}{\partial r} + \frac{1}{r}\sigma_{rz}^{\mathrm{tot}} = 0. \tag{62c}$$

As we mentioned earlier, due to the small value of the vacuum permittivity ε_0, the free-space stress is neglected. Moreover, under the constraint of incompressibility the total Piola-Kirchhoff stress becomes

$$\boldsymbol{S}^{\mathrm{tot}} = 2\frac{\partial\Psi}{\partial\boldsymbol{C}} + p\,\boldsymbol{C}^{-1}. \tag{63}$$

Sometimes, it is more convenient to derive the Cauchy-type total stress from the Piola-Kirchhoff stress $\boldsymbol{\sigma}^{\mathrm{tot}} = \boldsymbol{F}\boldsymbol{S}^{\mathrm{tot}}\boldsymbol{F}^T$. Using the expressions of the total anisotropic energy function in (50) and the deformation gradient defined in (60), the non-zero stress components of $\boldsymbol{\sigma}^{\mathrm{tot}}$ become

$$\begin{aligned}
\sigma_{\phi\phi}^{\mathrm{tot}} &= p + 2\lambda^2\Big[\Omega_1 + \Omega_2[\lambda^{-2}\lambda_z^{-2} + \lambda_z^2]\Big] - 2\Omega_5\lambda^{-2}\mathbb{E}_\Phi^2 - 4\Omega_6\lambda^{-4}\mathbb{E}_\Phi^2 \\
&\quad + \sum_{s=1}^{\mathrm{nid}}\rho^s[\tilde{\mu} + 2c_1E_s^2]\lambda^2[r_\theta^s]^2w^s \\
\sigma_{zz}^{\mathrm{tot}} &= p + 2\lambda_z^2\Big[\Omega_1 + \Omega_2[\lambda^{-2}\lambda_z^{-2} + \lambda^2]\Big] - 2[\Omega_5 + 2\Omega_6\lambda_z^{-2}]\lambda_z^{-2}\mathbb{E}_Z^2 \\
&\quad + \sum_{s=1}^{\mathrm{nid}}\rho^s[\tilde{\mu} + 2c_1E_s^2]\lambda^2[r_z^s]^2w^s \\
\sigma_{rr}^{\mathrm{tot}} &= p + 2\lambda^{-2}\lambda_z^{-2}\Big[\Omega_1 + \Omega_2[\lambda^2 + \lambda_z^2]\Big] - 2[\Omega_5 + 2\Omega_6\lambda^2\lambda_z^2]\lambda^2\lambda_z^2\mathbb{E}_R^2 \\
&\quad + \sum_{s=1}^{\mathrm{nid}}\rho^s[\tilde{\mu} + 2c_1E_s^2]\lambda^2[r_r^s]^2w^s \\
\sigma_{rz}^{\mathrm{tot}} &= -2\mathbb{E}_R\mathbb{E}_Z\Big[\Omega_5 + \Omega_6[\lambda^2\lambda_z^2 + \lambda_z^{-2}]\Big],
\end{aligned} \tag{64}$$

where $\boldsymbol{r} = \{r_r, r_\theta, r_z\}^T$.

4.2.2. Axially applied electric field

Among other ways to apply an electric field in this classical problem, the application of an axially applied field is discussed in the electro- and magneto-elasticity literature, see [8, 9, 19, 20]. Without considering the surrounding free space and after rearranging Eqn (62a) we obtain

$$\sigma_{rr}^{\text{tot}}(\bar{r}) = \int_{a_i}^{\bar{r}} \frac{1}{r}\Big[\sigma_{\theta\theta}^{\text{tot}}(r) - \sigma_{rr}^{\text{tot}}(r)\Big]\mathrm{d}r + q, \tag{65}$$

where q is an integration constant which can be determined from the boundary conditions for the stress. If the outer surface of the tube is free of mechanical loads we find

$$\begin{aligned} q &= -\int_{a_i}^{a_e} \frac{1}{r}\Big[\sigma_{\theta\theta}^{\text{tot}}(r) - \sigma_{rr}^{\text{tot}}(r)\Big]\mathrm{d}r + \sigma_{rr}^{\max}(a_e) \\ &= \int_{a_i}^{a_e} \frac{1}{r}\Big[\sigma_{rr}^{\text{tot}}(r) - \sigma_{\theta\theta}^{\text{tot}}(r)\Big]\mathrm{d}r + \sigma_{rr}^{\max}(a_e). \end{aligned} \tag{66}$$

At the inner boundary, the tube is subjected to a uniform pressure P

$$\sigma_{rr}^{\text{tot}}(a_i) = \sigma_{rr}^{\max}(a_i) - P, \tag{67}$$

that leads to

$$\begin{aligned} \sigma_{rr}^{\text{tot}}(a_i) &= \int_{a_i}^{a_i} \frac{1}{r}\Big[\sigma_{\theta\theta}^{\text{tot}}(r) - \sigma_{rr}^{\text{tot}}(r)\Big]\mathrm{d}r + q \\ &= \int_{a_i}^{a_e} \frac{1}{r}\Big[\sigma_{rr}^{\text{tot}}(r) - \sigma_{\theta\theta}^{\text{tot}}(r)\Big]\mathrm{d}r + \sigma_{rr}^{\max}(a_e) = \sigma_{rr}^{\max}(a_i) - P. \end{aligned} \tag{68}$$

The axially applied electric field will produce electric field lines which will be ideally aligned parallel to the longitudinal axis of the tube. Thus, the field lines will not depend on the tube radius. As a result, the influence of the field in the inner and outer surfaces are almost the same, i.e., $\sigma_{rr}^{\max}(a_i) = \sigma_{rr}^{\max}(a_e)$. This condition will yield

$$P = \int_{a_i}^{a_e} \frac{1}{r}\Big[\sigma_{\theta\theta}^{\text{tot}}(r) - \sigma_{rr}^{\text{tot}}(r)\Big]\mathrm{d}r. \tag{69}$$

We put the expressions of the stress components $\sigma_{\theta\theta}$ and σ_{rr} from Eqns (64) into the Eqn (69). After lengthy and rigorous calculations, which we skip writing here due to space constraint, the closed form results of the

pressure P can be expressed as

$$
\begin{aligned}
P = & \frac{\mu(I_4)}{\lambda_z}\left[\ln\left(\frac{\lambda_i}{\lambda_e}\right) - \frac{1}{2\lambda_z}\left[\lambda_i^{-2} - \lambda_e^{-2}\right]\right] \\
& + \frac{1}{2}\lambda_z^{-1}\left[\frac{\lambda_z\lambda_i^2 - 1}{\lambda_z\lambda_e^2 - 1}\right]\sum_{s=1}^{\text{nid}} \rho^s\, \tilde{\mu}\, w^s [r_\theta^s]^2 \\
& - \left[\lambda_z^{-1}\ln\left(\frac{\lambda_e}{\lambda_i}\right) + \frac{1}{2}\lambda_z^{-2}[\lambda_i^{-2} - \lambda_e^{-2}] + \frac{1}{2}\lambda_z^{-1}\left[\frac{\lambda_z\lambda_i^2 - 1}{\lambda_z\lambda_e^2 - 1}\right]\right]\sum_{s=1}^{\text{nid}} \rho^s\, \tilde{\mu}\, w^s [r_r^s]^2 \\
& + \frac{1}{2}\lambda_z^{-1}\left[\frac{\lambda_z\lambda_i^2 - 1}{\lambda_z\lambda_e^2 - 1}\right]\sum_{s=1}^{\text{nid}} 2\rho^s\, c_1\, [E_s]^2\, w^s [r_\theta^s]^2 \\
& - \left[\lambda_z^{-1}\ln\left(\frac{\lambda_e}{\lambda_i}\right) + \frac{1}{2}\lambda_z^{-2}[\lambda_i^{-2} - \lambda_e^{-2}] + \frac{1}{2}\lambda_z^{-1}\left[\frac{\lambda_z\lambda_i^2 - 1}{\lambda_z\lambda_e^2 - 1}\right]\right]\sum_{s=1}^{\text{nid}} 2\rho^s\, c_1\, [E_s]^2\, w^s [r_r^s]^2
\end{aligned}
\tag{70}
$$

where $\lambda_i = a_i/A_i, \quad \lambda_e = a_e/A_e$. In order to express the electric field-dependent shear modulus, we borrow the arguments of a field-dependent linear shear function from Bustamante [8] and Mehnert et al. [45] in the case of electro-elastic modelling, i.e., $\mu(I_4) = g_0 \pm I_4 g_1$, where g_0, g_1 are material constants.

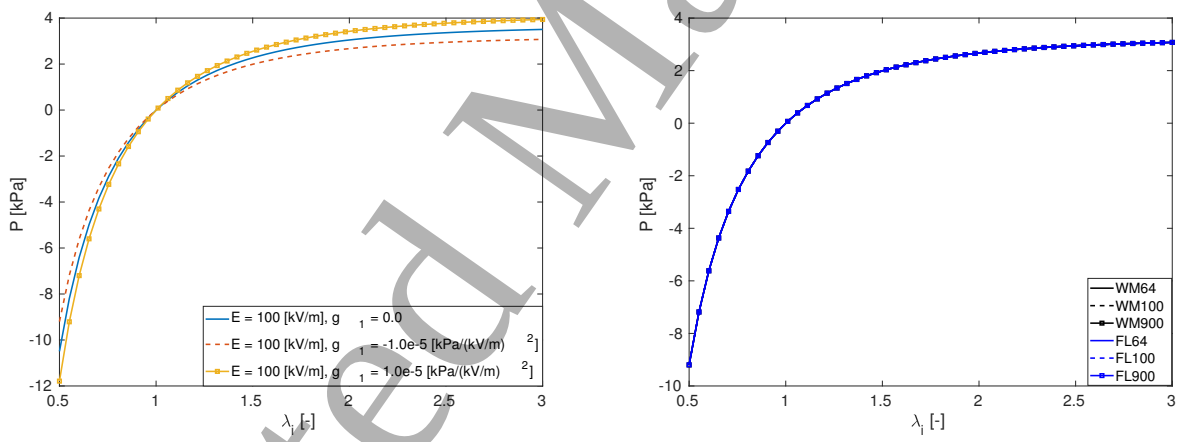

Figure 7: Plot of pressure over tube inflation λ_i for selected values of $\zeta = 2, \lambda_z = 1, b = 2.0$; a) Influence of the electric field on the pressure, b) Convergence test for various integration schemes

In order to illustrate few basic features of the non-homogeneous example, we at first concentrate to quantitatively reproduce some results with the help of the newly proposed model that are already available in the literature. For the material parameters appearing in the model, we take the values that are already identified in the previous section except the dispersion parameter b. Due to scarcity of experimental evidence, we follow an ansatz for the field dependence of the shear modulus $\mu(I_4)$ which is in line with an assumption already taken in the literature, cf. Bustamante [8], Mehnert et al. [42, 43]. They assume that the field-dependent shear modulus can be expressed via $\mu(I_4) = g_0 + g_1 I_4$, where g_1 is a negative scaling parameter and g_0 is the ground state shear modulus which is already identified, i.e. $g_0 = 0.81$kPa. The scaling parameter g_1 will be either negative or positive depending on the fact whether the shear modulus is increasing or

reducing by the applied electric field. Since we don't have enough experimental evidence at this moment, both possibilities are taken into account in this sequel, i.e. $\mu(I_4) = g_0 \pm g_1 I_4$. However, this ansatz can easily be fixed whenever more appropriate and illustrative experimental data will be available. Table 1 summarises three major parameters (two of them are identified in the previous section) with their appropriate units where the microscopic and macroscopic coupling parameters, c_1 and c_m, respectively, are related to $c_1 = 3c_m$. We prescribe an axial stretch characterised by λ_z, a radial inflation or contraction expressed by λ_i i.e. a ratio to the actual radius after the deformation to the initial radius. In addition to the mechanical stretch, the electric field is applied in the axial direction that is designated by E_Z, i.e. $\mathbb{E} = \{0, 0, E_Z\}^T$. For given values of the tube thickness ratio ζ, the axial stretch ratio λ_z and a fixed dispersion parameter $b = 2.0$, the applied pressure P vs λ_i is plotted in Fig (7a) to show the influence of the electric field on the pressure response captured by the model. Note that Figure (7a) depicts similar results to those produced by other models, cf. Mehnert et al. [45, 46], Bustamante [8]. It shows that the applied electric field softens the material response. For the tube inflation ($\lambda_i > 1$), a positive pressure has to be applied on the internal surface of the thick-walled tube. It reveals the pressure increases with the increasing value of the inflation. These results quantitatively match with the published figures in the literature, see [8, 45], Bustamante [8].

The isotropic as well as anisotropic parts of the energy function of the proposed constitutive framework is an electro-mechanical coupled extension of the neo-Hookean energy function. The internal pressure is almost maintained in higher inflations of the tube since at this point, the tube becomes so thin to take any inflation pressure further. The limitation of the neo-Hookean model for rubber elasticity is well known. As the inflation ratio (λ_i) becomes larger and larger, there is an upper limit of the pressure P that tends to an asymptotic value. This result is consistent with the results obtained by Melnikov & Ogden [83], Bustamante [8], Mehnert et al. [42,43] with isotropic as well as transverse anisotropic constitutive models that are inspired by a neo-Hookean formulation. However, if we take other advanced forms of energy functions, e.g. Gent model, the pressure will increase monotonically and for the Ogden model, it will be a maximum in the pressure followed by a minimum and subsequent monotonic increase as the inflation λ_i increases, see Melnikov & Ogden [83] for isotropic electro-active polymer modelling. Moreover, in the case of radial contraction ($\lambda_i < 1$), a negative pressure requires which decreases with the smaller value of λ_i.

For the numerical integration over the unit sphere, there are several integration schemes available in the literature. One of the key, but still much debated, questions is which numerical scheme is better suited for what type of constitutive model. Several research publications are dedicated to answer this pressing question in various areas, e.g. biological tissues, see for example, Ehret et al. [24], Verron [73], Itskov [36]. One of the simplest and most often used integration scheme, particularly in the case of isotropic modelling approach, is due to Bazant & Oh [6]. However several studies indicate that this simple and computationally efficient scheme yields unreliable results in the case of anisotropic models, cf. Ehret et al. [24], Verron [73]. We initially use this scheme, due to its simple computational cost with a symmetry property, however, since it produces unreliable results, alternative integration schemes are used later on. According to Itskov [36], Verron [73], Ehret et al. [24], the integration schemes proposed by Fliege & Maier [26], Womersley [83] can yield reliable results for anisotropic models. We compare Womersley integration scheme with Fliege & Maier scheme for various integration points, see Fig (7b). Interestingly, both schemes show consistent results even for the non-homogeneous tube example. Moreover, when we compare with different integration points of Womersley and Fliege & Maier, they end up with almost the same results. Henceforth, we confine ourself to the 64-point integration scheme from Womersley. A complete analysis of various integration schemes in the case of particle-filled anisotropic EAP models should be an interesting topics to explore

which will be a subject of investigation in our future contributions.

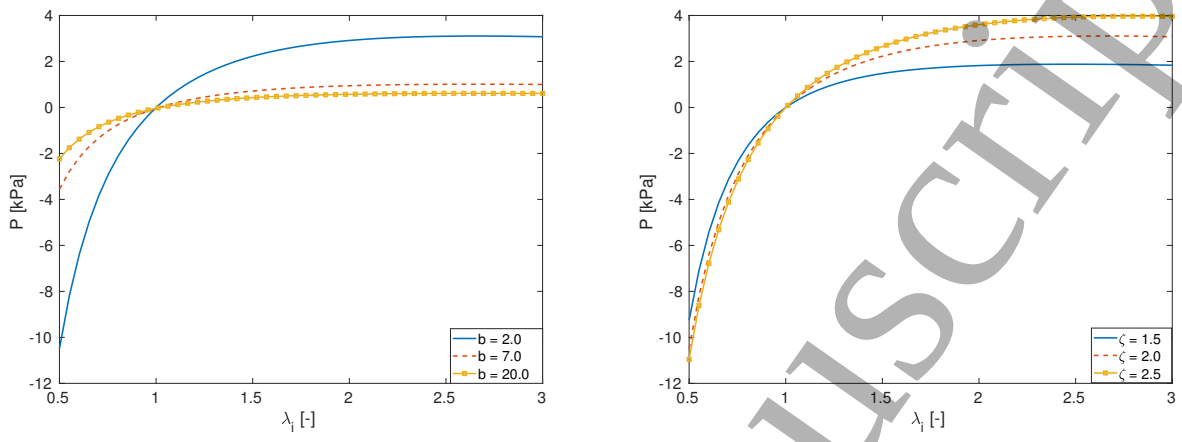

Figure 8: Plot of pressure over inflation λ_i for selected values of $\lambda_z = 1$, $E = 100$ kV/m; a) Variation with respect to the anisotropy parameter b and $\zeta = 2$, b) Variation with respect to the tube thickness ratio ζ when $b = 2.0$

Table 1: Various baseline material constants used in the tube problem.

$g_0 = \mu$ [kPa]	g_1 [kPa/[kV/m]^2]	c_m [F/m]
0.81	1.0×10^{-5}	3.25×10^{-14}

Similar to Bustamante [8] for the magneto-mechanical case and Mehnert et al. [45, 46] for the thermo-electro-mechanical case, the tube inflation pressure is plotted over the radial inflation λ_i for three different values of the degree of anisotropy $b = [2.0, 7.0, 20.0]$ in Fig (8a). As expected when the fibres are perfectly aligned ($b = 20.0$) in the direction of the applied electric field, the pressure will be minimum since there will be no contributions of the fibres in the azimuthal direction. In the case of $b = 2.0$ (solid line), some fibres are also aligned azimuthally which hinder the inflation in the circumferential direction that eventually results in larger pressure. A similar explanation for this non-homogeneous problem can be found in Gasser et al. [28] for the case of dispersed biological tissue modelling. Next, we present the pressure variation with respect to the tube thickness ζ, i.e. the ratio of the external to the internal radius. It is clear that for a given amount of inflation λ_i, a larger pressure is required with increasing tube thickness ζ. For a certain value of the anisotropy parameter, $b = 2.0$, the variation of the internal pressure for different thickness ratio is plotted in Fig (8b) which depicts that more inflation λ_i will yield similar results as in the case of increasing tube thickness ζ.

As mentioned earlier, the thickness of the tube is characterised by ζ, i.e. the ratio of the external to the internal radius. In Figure (9) it can be observed that the internal pressure decreases when the cylinder is stretched in the axial direction which is due to the decrease in the wall thickness of the cylinder as its volume is preserved thanks to the incompressibility constraint. This reduction of the pressure is more pronounced in the case of smaller values of the dispersion parameter b, i.e., when some chains align in the circumferential direction the pressure will be more and the reduction will be prominent, see Fig (9a). For a given value of the anisotropy parameter, $b = 2.0$, the variation of the internal pressure for different thickness ratio is

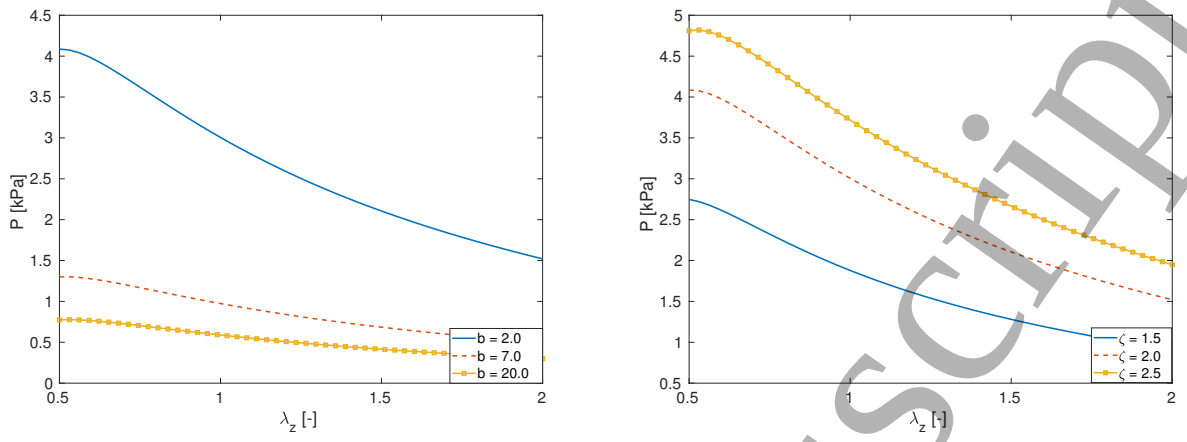

Figure 9: Plot of pressure to illustrate the dependence on the axial stretch for selected values of $\lambda_i = 2.0$, $E = 100$ kV/m; a) Pressure variation due to various dispersion values b, b) Pressure with respect to the tube thickness ratio ζ when $b = 2$

plotted in Fig (9b). However, when the initial tube thickness ζ is changed, the magnitude of the pressure is affected accordingly, i.e. the pressure reduction in a thicker tube is more prominent than a relatively thin tube, see Fig (9b).

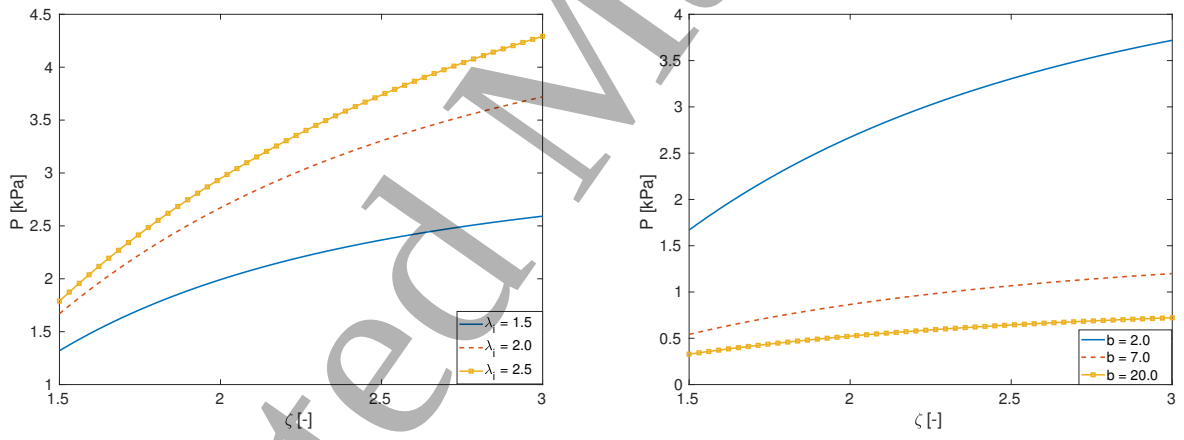

Figure 10: Variation of pressure over tube thickness for selected values of $\lambda_z = 1$, $E = 100$ kV/m; a) Pressure dependence with respect to inflation for a given anisotropy parameter $b = 2.0$, b) Pressure with respect to various dispersion parameters b but for a fixed inflation value of $\lambda_i = 2$

Similar to the tube inflation, the pressure will increase under an increasing value of the tube thickness ratio. If we increase the inflation ratio, it will yield more pressure, cf Fig (10a). Figure (10b) reveals that in the case of dispersed chain characterised by smaller value of b, the pressure will increase in a similar manner as in the case of greater inflation ratio.

Next we investigate the variation of the pressure with respect to the electric field strength E for various inflation ratio and the degree of dispersion b. Figure (11a) shows that the tube pressure drops with the increasing magnitude of the applied electric field. This is due to the fact that the applied field softens the material

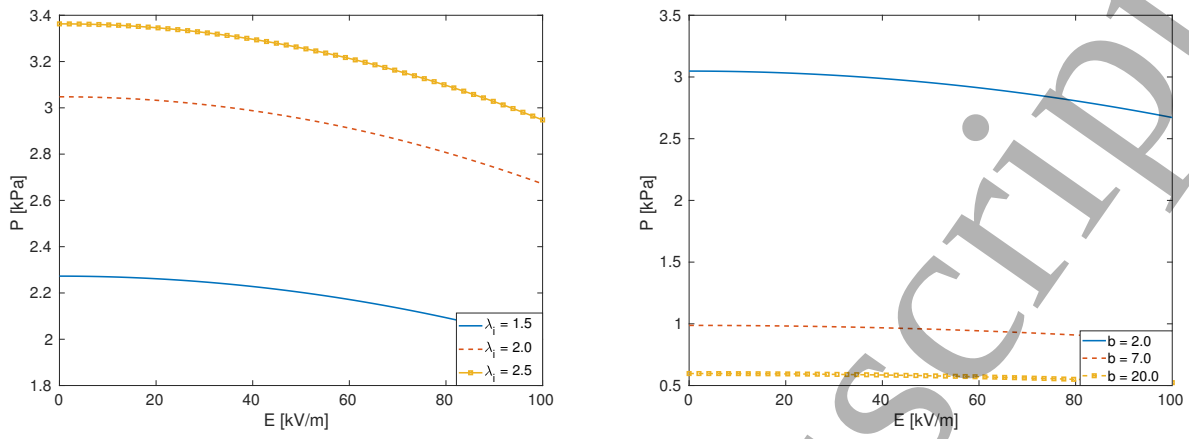

Figure 11: Pressure dependence on the electric field for selected values of $\lambda_z = 1, \zeta = 2$; a) Variation with respect to the radial inflation for a dispersion parameter $b = 2.0$, b) Variation with respect to different dispersion parameters for an inflation value of $\lambda_i = 2$

which is scaled by the field-dependent shear function $\mu(I_4)$. For the dispersion captured by the parameter b, its smaller value ($b = 2.0$) will yield larger pressure since some chains will align in the azimuthal direction. Moreover, the softening effect is more vivid when the major chains are in the circumferential direction compared to the perfectly aligned chains in the axial direction, i.e. $b = 20$, cf Fig (11b).

5. Conclusion and outlook

In this contribution a dispersion-type anisotropic constitutive framework for EAPs is proposed. In an attempt to improve actuation mechanisms, high permittivity particles are used in a polymeric matrix to manufacture EAP composites. For further improvements in the actuation, an electric field is applied during the curing process of the composites which form transversely anisotropic polymers with a dispersion along a mean orientation axis. The proposed constitutive model captures the chain dispersion anisotropy with a probability distribution function in integral form. To obtain the results in discrete form, some advanced integration schemes over the unit micro-sphere are utilised. Several homogeneous and non-homogeneous benchmark examples demonstrate that the presented formulations correctly capture relevant phenomena in transversely isotropic electro-elastic polymeric materials with a chain dispersion. The underlying bulk polymeric materials in EAP composites are typically viscoelastic. Hence, a time-dependent viscoelastic extension of the proposed model will be treated in our forthcoming contributions. Moreover, for simulations with more realistic boundary value problems, the proposed model needs to be implemented into a finite element code which will be addressed in another contribution. A comparison between the AI-based approach and the GST-inspired approach for electro-mechanically coupled problems is a tempting work to perform in the future. We have a plan to identify the dispersion parameter b of the proposed constitutive framework with experimental data of particle-filled EAPs.

Acknowledgements:

The second author acknowledges the funding by the DFG Cluster of Excellence : Engineering of Advanced Materials (EAM) and project no. STE 544/52-1.

References:

[1] Alastrue V, M Martinez, M Doblare, A Menzel, Anisotropic micro-sphere-based finite elasticity applied to blood vessel modeling, International Journal of Mechanics and Physics of Solids, 57:178-203, 2009

[2] Alastrue V, M Martinez, A Menzel, M Doblare, On the use of non-linear transformations for the evaluation of anisotropic rotationally symmetric integrals, International Journal of Numerical Methods in Engineering, 79:474-504, 2009

[3] Alastrue V, P Saez, M Martinez, M Doblare, On the use of Bingham statistical distribution in microsphere-based constitutive models for arterial tissue, Mechanics Research Communications, 37:700-706, 2010

[4] Ask A, A. Menzel, M. Ristinma, Phenomenological modeling of viscous electrostrictive polymers, International Journal of Non-Linear Mechanics, 47(2):156-165, 2012

[5] Brochu P, Pei Q, Advances in dielectric elastomers for actuators and artificial muscles, Macromolecular Rapid Communications 31:10-36, 2010

[6] Bazant Z P, Oh B H, Efficient numerical integration on the surface of a sphere, Z. Angew. Math. Mech.66:37-49, 1986

[7] Büschel A, S. Klinkel and W. Wagner, Dielectric elastomers- Numerical modeling of nonlinear viscoelasticity, International Journal of Numerical Methods in Engineering 93:834-856, 2013

[8] Bustamante R, Transversely isotropic nonlinear magneto-active elastomers, Acta Mechanica, 210(3-4):183-214, 2010

[9] Bustamante B, Transversely isotropic nonlinear electro-active elastomers, Acta Mechanica, 206(3-4):237-259, 2009

[10] Bustamante R, A variational formulation for a boundary value problem considering an electro-sensitive elastomer interacting with two bodies, Mechanics Research Communication, 36 (7):791-795, 2009

[11] Carpi F, D. De Rossi, Improvement of electromechanical actuating performances of a silicone dielectric elastomer by dispersion of titaniun dioxide powder, IEEE Trans Dielectr Electr Insul, 12:835-843, 2005

[12] Carpi F, G. Gallone, F. Galantini, D. De Rossi, Silicone-poly(hexylthiophene) blends as elastomers with enhanced electromechanical transduction properties, Adv Funct Mater, 18:235-241, 2008

[13] Carpi F, Chiarelli P, Mazzoldi A, Rossi D D, Electromechanical characterisation of dielectric elastomer planar actuators: comparative evaluation of different electrode materials and different counter-loads, Sensors and Actuators A: Physical, 107(1):85 - 95, 2003.

[14] Cortes D H, S. P. Lake, J. A. Kadlowec, L. J. Soslowsky, D. M. Elliot, Characterizing the mechanical contribution of fiber angular distribution in connective tissue: comparison of two modeling approaches, Biomech Model Mechanobiol, 9:651-658, 2010

[15] Cortes D H, D. M. Elliot, Modelling of collagenous tissues using distributed fiber orientations, Structure-based mechanics of tissues and organs, pp.15-38, (Kassab and Sacks edited), Springer, 2016

[16] Cortes D H, D. M. Elliot, Accurate prediction of stress in fibers with distributed orientations using generalized high-order structure tensors, Mechanics of Materials, 75:73-83, 2014

[17] Dorfmann A and R.W. Ogden, Nonlinear electroelasticity, Acta Mechanica, 174(3):167-183, 2005

[18] Dorfmann A and R.W. Ogden, Nonlinear electroelastic deformations, Journal of Elasticity, 82(2):99-127, 2006

[19] Dorfmann A, R. W. Ogden, Nonlinear magnetoelastic deformations, Quarterly Journal of Mechanics and Applied Mathematics, 57(4):599-622, 2004

[20] Dorfmann A, R. W. Ogden, Some problems in nonlinear magnetoelasticity, ZAMP, 56(4):718-745, 2005

[21] Dorfmann L, Ogden R W, Nonlinear electroelasticity : material properties, continuum theory and applications. Proceedings of the Royal Society/ A, 473, 20170311, 2017

[22] Diaconu I, D.O. Dorohoi and C. Ciobanu, Eletromechanical response of polyurethane films with different thickness, Romanian Journal of Physics, 53(1-2):91-97, 2008

[23] Dang Z M, J K Yuan, J W. Zha, T Zhou, S T Li, G H Hu, Fundamentals, processes and applications of high-permittivity polymer-matrix composites, Prog Mater Sci, 57:660-723,2012

[24] Ehret A E, M Itskov, H Schmid, Numerical integration on the sphere and its effect on the material symmetry of constitutive equations- a comparative study, International Journal of Numerical Methods in Engineering, 81:189-206, 2010

[25] Etse G, M Nieto, P Steinmann, A micropolar microplane theory, International Journal of Engineering Science, 41(13-14):1631-1648, 2003

[26] Fliege J, Maier U, The distribution of points on the sphere and corresponding cubature formulae. IMA Journal of Numerical Analysis 19(2):317-334, 1999

[27] Gallone G, Carpi F, Rossi D D, Levita G, Marchetti A, Dielectric constant enhancement in a silicone elastomer filled with lead magnesium niobate-leads titanate, Materials Science and Engineering C 27:110-1162, 2007

[28] Gasser T C, R W Ogden, G A Holzapfel, Hyperelastic modelling of arterial layers with distributed collagen fibre orientations, J. R. Soc. Interface, 3(6): 15-35, 2006

[29] Gao Z, A. Tuncer, A. H. Cuitino, Modeling and simulation of the coupled mechanical-electrical response of soft solids, International Journal of Plasticity, 27(10):1459-1470, 2011

[30] Hossain M, Saxena P, Steinmann P, Modelling the mechanical aspects of the curing process of magneto-sensitive elastomeric materials, International Journal of Solids and Structures 58: 257-269, 2015

[31] Hossain M, Chatzigeorgiou G, Meraghni F, Steinmann P, A multi-scale approach to model the curing process in magneto-sensitive polymeric materials, International Journal of Solids and Structures, 69-70:34-44, 2015

[32] Hossain M, Steinmann P, More hyperelastic models for rubber-like materials: Consistent tangent operator and comparative study, Journal of the Mechanical Behaviour of Materials 22(1-2):27-50, 2013

[33] Hossain M, N Kabir, A F M S Amin, Eight-chain and full-network models and their modified versions for rubber hyperelasticity : A comparative study, Journal of the Mechanical Behaviour of Materials, 24(1-2):11-24, 2015

[34] Hossain M, D. K. Vu, P. Steinmann, Experimental study and numerical modelling of VHB 4910 polymer, Computational Materials Science, 59:65-74, 2012

[35] Hossain M, D. K. Vu, P. Steinmann, A comprehensive characterization of the electro-mechanically coupled properties of VHB 4910 polymer, Archive of Applied Mechanics, 85(4):523-537, 2014

[36] Itskov M, On the accuracy of numerical integration over the unit sphere applied to full network models, Computational Mechanics, 57(5):859-865, 2016

[37] Johlitz M, H. Steeb, S. Diebels, A. Chatzouridou, J. Batal and W. Possart, Experimental and theoretical investigation of nonlinear viscoelastic polyurethane systems, Journal of Materials Science, 42:9894-9904, 2007

[38] Koh S J A, C. Keplinger, T. Li, S. Bauer, Z. Suo, Dielectric elastomer generators: How much energy can be converted?, Mechatronics, IEEE/ASME Transactions , 33-41, 16(1), 2011.

[39] Kashani M R , S. Javadi, N. Gharavi, Dielectric properties of silicone rubber-titanium dioxide composites prepared by dielectrophoretic assembly of filler particles, Smart Materials and Structures, 19:1-7, 2010

[40] Kussmaul B, Risse S, Kofod G, Wache R, Wegener M, McCarthy DN, Krueger H and Gerhard R, Enhancement of dielectric permittivity and electromechanical response in silicone elastomers: Molecular grafting of organic dipoles to the macromolecular network, Advanced Functional Materials 21:4589-4594, 2011

[41] Kuhl E, P Steinmann, I Carol, A thermodynamically consistent approach to microplane theory. Part II. Dissipation and inelastic constitutive modeling, International Journal of Solids and Structures, 38:2933-2952, 2001

[42] Keip M A, Steinmann P, Schröder J, Two-scale computational homogenization of electro-elasticity at finite strains, Computer Methods in Applied Mechanics and Engineering 278: 62-79, 2014

[43] Kollosche M, Zhu J, Suo Z, Kofod G, Complex interplay of nonlinear processes in dielectric elastomers, Physical Review E 85:051801, 2012

[44] Liu B, Shaw M T, Electrorheology of filled silicone elastomers, Journal of Rheology 45:641-657,2011

[45] Mehnert M, M Hossain, P Steinmann, On nonlinear thermo-electro-elasticity, Proceedings of the Royal Society/ A, 472 (2190), 20160170, 2016

[46] Mehnert M, M Hossain, P Steinmann,Towards a thermo-magneto-mechanical coupling framework for magneto-rheological elastomers, International Journal of Solids and Structures, 2017, doi.org/10.1016/j.ijsolstr.2017.08.022

[47] Monk P, Finite Element Methods for Maxwell Equations, Oxford University Press, Clarendon (2003)

[48] Ma W, L. E. Cross, An experimental investigation of electromechanical response in a dieletric acrylic elastomer, Applied Physics A, 78:1201-1204, 2004

[49] Michel S, X. Q. Zhang, M. Wissler, C. Löwe, G. Kovocs, A comparison between silicone and acrylic elastomers as dielectric materials in electroactive polymer actuators, Polymer International, 59:391-399, 2010

[50] Molberg M, D. Crespy, P. Rupper, F. Nesch, J.A.E. Manson, C. Loewe, D.M. Opris, High breakdown field dielectric elastomer actuators using encapsulated polyaniline as high dielectric constant filler, Adv Funct Mater, 20: 3280-3291, 2010

[51] Miehe C, S. Göktepe and F. Lulei, A Micro-macro approach to rubber-like materials: Part-I, the non-affine micro-sphere model of rubber elasticity, Journal of the Mechanics and Physics of Solids, 52:2617-2660, 2004

[52] Miehe C and S. Göktepe, A micro-macro approach to rubber-like materials: Part-II, the micro-sphere model of finite rubber viscoelasticity, Journal of the Mechanics and Physics of Solids, 53:2231-2258, 2005

[53] Ogden, R W, 1997. Non-linear Elastic Deformations, Dover, New York.

[54] Gil A G, R. Ortigosa, A new framework for large strain electromechanics based on convex multi-variable strain energies: Variational formulation and material characterisation, Computer Methods in Applied Mechanics and Engineering, 302: 293-328, 2016

[55] Ortigosa R, Antonio G Gil, A new framework for large strain electromechanics based on convex multi-variable strain energies: Finite Element discretisation and computational implementation, Computer Methods in Applied Mechanics and Engineering, 302 : 329-360, 2016

[56] Pandolfi A, M Vasta, Fiber distributed hyper elastic modelling of biological tissues, Mechanics of Materials,44:151-162, 2012

[57] Vasta M, A Gizzi, A Pandolfi, On three- and two-dimensional fiber distributed models of biological tissues, Probabilistic Engineering Mechanics, 37:170-179, 2014

[58] Pelteret J P, D Davydov, A McBride, D K Vu, P Steinmann, Computational electro- and magneto-elasticity for quasi-incompressible media immersed in free space, International Journal for Numerical Methods in Engineering, 108 (11): 1307-1342, 2016

[59] Qiang J , H. Chen and B. Li, Experimental study on the dielectric properties of polyacrylate dielectric elastomer, Smart Material Structures, 21:1-9, 2012

[60] Risse S, B. Kussmaul, H. Krueger, G. Kofod Synergistic improvement of actuation properties with compatibilized high permittivity filler, Adv Funct Mater, 22: 3958-3962, 2012

[61] Risse S, B. Kussmaul, H. Krueger, G. Kofod, A versatile method for enhancement of electromechanical sensitivity of silicone elastomers, RSC Adv, 2: 9029-9035, 2012

[62] Steinmann P, M Hossain, G Possart, Hyperelastic models for rubber-like materials: Consistent tangent operators and suitability of Treloar's data, Archive of Applied Mechanics, 82(9):1183-1217, 2012

[63] Spencer A J M, Theory of invariants, in: Eringen, A. C. (ed.) Continuum Physics, Vol 1. Academic, New York, pp 239-353, 1971

[64] Saxena P, M Hossain, P Steinmann, A theory of finite deformation magneto-viscoelasticity, International Journal of Solids and Structures, 50(24):3886-3897, 2013

[65] Saxena P, D K Vu, P Steinmann, On rate-dependent dissipation effects in electro-elasticity, International Journal of Non-Linear Mechanics, 62:1-11, 2014

[66] Saxena P, J P Pelteret, P Steinmann, Modelling of iron-filled magneto-active polymers with a dispersed chain-like microstructure, European Journal of Mechanics-A/Solids 50: 132-151, 2015

[67] Skacel P, J Bursa, Comparison of constitutive models of arterial layers with distributed collagen fibre orientations, Acta of Bioengineering and Biomechanics, 16(3):47-58, 2014

[68] Skacel P, J Bursa, Numerical implementation of constitutive model of arterial layers with distributed collagen fibre orientations, Computer Methods of Biomechanics and Biomedical Engineering,18(8):816-828, 2015

[69] Skatulla S, C Sansour, A Arockiarajan, A multiplicative approach for nonlinear electro-elasticity, Computer Methods in Applied Mechanics and Engineering, 245-246:243-255, 2012

[70] Tomer V, C.A. Randall, High field dielectric properties of anisotropic polymer-ceramic composites, J Appl Phys, 104: 074106/1-7, 2008

[71] Thylander S, Microsphere-based modeling of electro-active polymers, PhD Dissertation, Lund University, Sweden, 2016

[72] Thylander S, A. Menzel and M. Ristinmaa, An electromechanically coupled micro-sphere framework : Application to the finite element analysis of electrostrictive polymers, Smart Materials and Structures 21, 094008, 2012

[73] Verron E, Questioning numerical integration methods for microsphere (and microplane) constitutive equations, Mechanics of Materials, 89:216-228, 2015

[74] Vogel F, On the modeling and computation of electro- and magneto-active polymers, PhD Dissertation, Friedrich-Alexander-University Erlangen-Nuremberg, Germany, 2014.

[75] Vogel F, S. Goektepe, E. Kuhl, P. Steinmann, Modeling and simulation of viscous electro-active polymers, European Journal of Mechanics A/Solids, 48:112-128, 2014

[76] Vogel F, R. Bustamante, P. Steinmann, On mixed variational principles in electro-elastostatics, International Journal of Non-linear Mechanics, 47:341-354, 2012

[77] Vertechy R , M. Fontana, G. R. Papini, D. Forehand, In-tank tests of a dielectric elastomer generator for wave energy harvesting, In SPIE Smart Structures and Materials- Nondestructive Evaluation and Health Monitoring, 90561G-90561G, International Society for Optics and Photonics, 2014

[78] Vu D K, P. Steinmann, Numerical modeling of Non-linear electroelasticity, International Journal for Numerical Methods in Engineering, 70:685-704, 2007

[79] Vu D K, P. Steinmann, A 2-D coupled BEM-FEM simulation of electro-elastostatics at large strain, Computer Methods in Applied Mechanics and Engineering, 199:1124-1133, 2010

[80] Wissler M, E. Mazza, Mechanical behavior of an acrylic elastomer used in dielectric elastomer actuators, Sensors and Actuators A, 134:494-504, 2007

[81] Yang Ta-I, Kofinas P, Dielectric properties of polymer nanoparticle composites, Polymer, 48:791-798, 2009

[82] Vo L T, Anastasiadis S P, Giannelis E P, Dielectric study of polystyrene-co-butadiene composites with carbon black, silica, and nanoclay, Macromolecules 44:6161-6171, 2011

[83] Womersley R S, Interpolation and Cubature on the Sphere- UNSW Sydney web.maths.unsw.edu.au/ rsw/Sphere/ (Accessed on 11 June 2017)

[84] Zäh D, C Miehe, Multiplicative electro-elasticity of electroactive polymers accounting for micromechanically-based network models, Computer Methods in Applied Mechanics and Engineering, 286:394-421, 2015

[85] Melnikov A, Ogden R W, Finite deformations of an electroelastic circular cylindrical tube. Zeitschrift fuer angewandte Mathamatik und Physik, ZAMP, 67:140, 2016

[86] Liu Y, Liu L, Yu K, Sun S, Leng J, An investigation on electromechanical stability of dielectric elastomer undergoing large deformation, Smart Materials and Structures, 18, 095040, 2009

[87] Liu Y, Liu L, Yu K, Zhang Z, Leng J, Dielectric elastomer film actuators: characterization, experiment and analysis. Smart Materials and Structures, 18, 095024, 2009

[88] Leng J, Liu L, Liu Y, Yu K, Sun S, Electromechanical stability of dielectric elastomer, Applied Physics Letters, 95(1), 211901, 2009

[89] Liu Y, Liu L, Yu K, Leng J, Thermoelectromechanical stability of dielectric elastomers undergoing temperature variation. Mechanics of Materials, 72, 33-45, 2014

[90] Liu Y, Liu L, Luo X, Li B, Leng J, Electromechanical instability and snap-through instability of dielectric elastomers undergoing polarization saturation. Mechanics of Materials, 55, 60-72, 2012